

Generalized Recorruped-to-Recorruped: Self-Supervised Learning Beyond Gaussian Noise

Brayan Monroy¹, Jorge Bacca¹, and Julian Tachella²

¹Universidad Industrial de Santander, Colombia

²CNRS, ENS de Lyon

<https://github.com/bemc22/GeneralizedR2R>

Abstract

Recorruped-to-Recorruped (R2R) has emerged as a methodology for training deep networks for image restoration in a self-supervised manner from noisy measurement data alone, demonstrating equivalence in expectation to the supervised squared loss in the case of Gaussian noise. However, its effectiveness with non-Gaussian noise remains unexplored. In this paper, we propose Generalized R2R (GR2R), extending the R2R framework to handle a broader class of noise distribution as additive noise like log-Rayleigh and address the natural exponential family including Poisson and Gamma noise distributions, which play a key role in many applications including low-photon imaging and synthetic aperture radar. We show that the GR2R loss is an unbiased estimator of the supervised loss and that the popular Stein’s unbiased risk estimator can be seen as a special case. A series of experiments with Gaussian, Poisson, and Gamma noise validate GR2R’s performance, showing its effectiveness compared to other self-supervised methods.

1 Introduction

Image restoration is essential in many scientific and engineering applications, from medical imaging to computational photography. State-of-the-art image restoration approaches train a deep network to predict clean images from noisy measurements. However, most approaches are based on supervised learning, which requires clean image datasets for effective deep network training [1]. This reliance introduces significant challenges, such as the scarcity of clean image data in many important medical and scientific imaging applications [2], and the risk of models overfitting or memorizing specific examples [3, 4]. As a result, there is growing interest in developing robust self-supervised learning strategies that can operate exclusively on noisy data [5, 6, 7], representing a promising direction for the future of image processing and computer vision.

Self-supervised image denoising has attracted significant attention for its potential to perform denoising without relying on clean, paired data, making it a baseline for many image restoration techniques. Methods in this domain are often classified based on the level of prior knowledge they require about the noise distribution [8].

The first class of methods relies on two independent noisy realizations per image to construct a loss that uses these pairs as inputs and targets. Noise2Noise [6] can obtain performance close to supervised learning, but obtaining independent noisy pairs is impossible in many applications. The second class only assumes that the noise distribution is independent across pixels. Blind Spot Networks, for example, rely on a masking strategy applied to the input or within the network itself [9, 10, 11]. This approach forces the network to predict denoised values based solely on neighboring pixels, leveraging the assumption of local spatial correlations within the image. As the central pixel is not used, these methods generally have suboptimal performance.

The third family of methods assumes that the noise distribution is fully known, and can obtain performances that are on par with supervised learning. Stein’s Unbiased Risk Estimator (SURE) [12] loss matches the supervised loss in expectation, and is available for Gaussian, Poisson [13] and Poisson-Gaussian noise distributions [13]. However, SURE requires approximating the divergence of the restoration function [14], which can lead to suboptimal results. The computation of the divergence is avoided by Noise2Score [15], which approximates the score of the noisy distribution during training and leverages Tweedie’s formula to denoise at the test time. Finally, Recorruped-to-Recorruped [7, 16] synthetically recorrupes a noisy image into noisy pairs, removing the need to approximate the divergence term, while remaining an unbiased estimator of the supervised loss. However, this method has been mostly demonstrated with Gaussian noise.

This work extends the R2R framework to address noise types beyond the traditional additive Gaussian model by introducing Generalized R2R (GR2R). Our formulation covers two noise modalities: additive noise and noise distributions within the natural exponential family. By generating independent noisy image pairs from a single noisy image following a specified noise distribution, we establish equivalence to supervised learning through traditional mean-square-error (MSE) loss. Additionally, we demonstrate that the GR2R approach can be seen as a generalization of the well-known SURE loss, which does not require the computation of divergences. We further propose using the negative log-likelihood loss that takes into account the noise distribution of the recorrputed measurements and show how the method can be adapted to tackle general inverse problems. The GR2R framework enables training any deep network for NEF noise distributions without requiring modifications to the network structure. We conduct simulations for Gaussian, Poisson, and Gamma noise distributions on image datasets where these distributions are particularly relevant, including magnetic resonance imaging (MRI), natural image denoising, and synthetic aperture radar (SAR). Results demonstrate that GR2R effectively handles diverse noise distributions, achieving a performance on par with fully supervised learning.

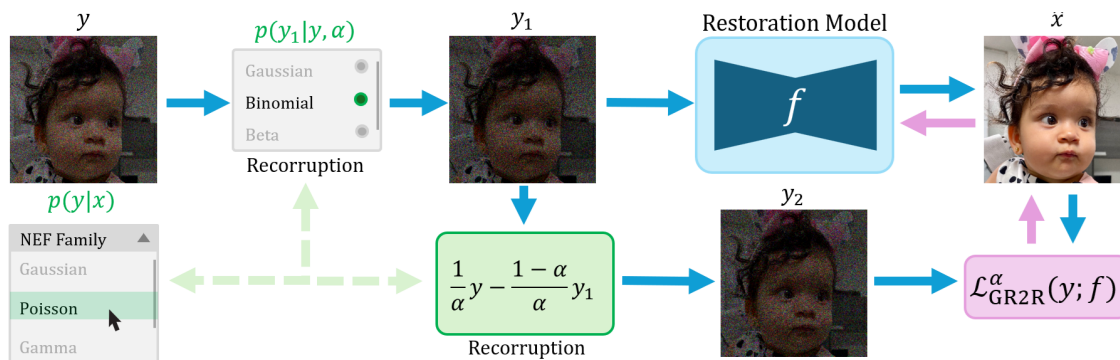


Figure 1: **Overview of GR2R framework.** Given a noisy image $\mathbf{y} \sim p(\mathbf{y}|\mathbf{x})$, which belongs to a NEF, GR2R generates pairs of independent noisy images \mathbf{y}_1 and \mathbf{y}_2 through additional recorrputation to enable self-supervised denoising learning $\hat{f}(\mathbf{y}_1) \approx \mathbb{E}\{\mathbf{x}|\mathbf{y}_1\}$.

2 Related Work

Supervised and Self-Supervised Learning. The goal of supervised learning is to learn a deep denoiser operator $\hat{\mathbf{x}} = \hat{f}(\mathbf{y})$ given noisy/clean paired data (\mathbf{y}, \mathbf{x}) . This process can be mathematically described by the minimization of the supervised loss function as follows

$$\hat{f} = \arg \min_f \mathbb{E}_{\mathbf{x}, \mathbf{y}} \mathcal{L}_{\text{SUP}}(\mathbf{x}, \mathbf{y}; f), \quad (1)$$

where $\mathcal{L}_{\text{SUP}}(\mathbf{x}, \mathbf{y}; f) = \|f(\mathbf{y}) - \mathbf{x}\|_2^2$, which is the MSE between the estimation and clean images¹. The optimal estimator is the Minimum MSE $\hat{f}(\mathbf{y}) \approx \mathbb{E}\{\mathbf{x}|\mathbf{y}\}$. In practice, the expectation is approximated with a finite dataset with N samples, i.e., $\frac{1}{N} \sum_{i=1}^N \mathcal{L}_{\text{SUP}}(\mathbf{x}^{(i)}, \mathbf{y}^{(i)}; f)$. By simple algebra manipulation \mathcal{L}_{SUP} can be split between unsupervised and supervised terms as follows

$$\mathcal{L}_{\text{SUP}}(\mathbf{x}, \mathbf{y}; f) = \|f(\mathbf{y}) - \mathbf{y}\|_2^2 + 2f(\mathbf{y})^\top (\mathbf{y} - \mathbf{x}) + \text{const.}$$

When there is no access to the set of clean images \mathbf{x} , self-supervised methods aim to approximate/eliminate the term that contains access to \mathbf{x} , $f(\mathbf{y})^\top (\mathbf{y} - \mathbf{x})$ by building a self-supervised loss $\mathcal{L}_{\text{SELF}}$ such that

$$\mathbb{E}_{\mathbf{y}|\mathbf{x}} \mathcal{L}_{\text{SELF}}(\mathbf{y}; f) = \mathbb{E}_{\mathbf{y}|\mathbf{x}} \mathcal{L}_{\text{SUP}}(\mathbf{x}, \mathbf{y}; f) + \text{const.} \quad (2)$$

¹It is important to highlight that other cost functions can be used, such as the mean absolute error.

Stein’s Unbiased Risk Estimator. Assuming that the measurements are corrupted by Gaussian noise, $\mathbf{y}|\mathbf{x} \sim \mathcal{N}(\mathbf{x}, \mathbf{I}\sigma^2)$ and f be weakly differentiable, SURE propose the following self-supervised loss

$$\mathcal{L}_{\text{SURE}}(\mathbf{y}; f) = \|\mathbf{f}(\mathbf{y}) - \mathbf{y}\|_2^2 + 2\sigma^2 \sum_{i=1}^n \frac{\partial f_i}{\partial y_i}(\mathbf{y}), \quad (3)$$

where the last term is the divergence of f at \mathbf{y} . Consequently, SURE guarantees that

$$\mathbb{E}_{\mathbf{y}|\mathbf{x}}\{f(\mathbf{y})^\top(\mathbf{y} - \mathbf{x})\} = \mathbb{E}_{\mathbf{y}|\mathbf{x}}\left\{\sigma^2 \sum_{i=1}^n \frac{\partial f_i}{\partial y_i}(\mathbf{y})\right\},$$

therefore, the SURE expectation loss serves as an unbiased risk estimator of its supervised counterpart, with $\hat{\mathbf{f}}(\mathbf{y}) \approx \mathbb{E}\{\mathbf{x}|\mathbf{y}\}$. Noteworthy advancements beyond Gaussian noise include the Hudson lemma [17], which extends SURE to the exponential family, and GSURE [18], which further extends it to non-i.i.d exponential families.

Noise2Void and Blind Spot Networks. Noise2Void methods and blind spot networks build constrained denoisers f that do not look at the central pixel for denoising, ie $\frac{\partial f_i}{\partial y_i}(\mathbf{y}) = 0$ for all $\mathbf{y} \in \mathbb{R}^n$ and $i = 1, \dots, n$. Then, a constrained network f can be trained on simple measurement consistency

$$\mathcal{L}_{\text{MC}}(\mathbf{y}; f) = \|\mathbf{f}(\mathbf{y}) - \mathbf{y}\|_2^2, \quad (4)$$

where, if the noise distribution is independent across pixels, i.e., $p(\mathbf{y}|\mathbf{x}) = \prod_{i=1}^n p(y_i|x_i)$, then we have that

$$\mathbb{E}_{\mathbf{y}|\mathbf{x}}\{f(\mathbf{y})^\top(\mathbf{y} - \mathbf{x})\} = 0.$$

Alternatively, approaches such as Neigh2Neigh [19, 20] design a custom loss function that removes the central pixel instead of using a blind spot denoiser. However, note that the learned network is not optimal for MMSE because $\hat{\mathbf{f}}(\mathbf{y}) \neq \mathbb{E}\{\mathbf{x}|\mathbf{y}\}$, due to the zero derivative constraint.

Noise2Noise. Assume a training set of paired noisy/noisy images is available. Specifically, the authors in [6] described the pairs of noisy images as

$$\mathbf{y}_1 \sim p(\mathbf{y}_1|\mathbf{x}), \quad \mathbf{y}_2 \sim p(\mathbf{y}_2|\mathbf{x}), \quad (5)$$

then, a denoiser operator f is adjusted to minimize the squared ℓ_2 loss

$$\mathcal{L}_{\text{N2N}}(\mathbf{y}_1, \mathbf{y}_2; f) = \|\mathbf{f}(\mathbf{y}_1) - \mathbf{y}_2\|_2^2, \quad (6)$$

since the noisy pairs are independent with $\mathbf{y}_1, \mathbf{y}_2$ independent conditioned on \mathbf{x} and $\mathbb{E}\{\mathbf{y}_1|\mathbf{x}\} = \mathbb{E}\{\mathbf{y}_2|\mathbf{x}\} = \mathbf{x}$, then the supervised term is reduced such that

$$\begin{aligned} & \mathbb{E}_{\mathbf{y}_1, \mathbf{y}_2|\mathbf{x}}\{f(\mathbf{y}_1)^\top(\mathbf{y}_2 - \mathbf{x})\} \\ &= \mathbb{E}_{\mathbf{y}_1|\mathbf{x}}f(\mathbf{y}_1)^\top \mathbb{E}_{\mathbf{y}_2|\mathbf{x}}(\mathbf{y}_2 - \mathbf{x}) = 0, \end{aligned}$$

hence, the Noise2Noise expectation loss closely matches its supervised counterpart $\mathbb{E}_{\mathbf{y}_1, \mathbf{y}_2|\mathbf{x}}\mathcal{L}_{\text{N2N}}(\mathbf{y}_1, \mathbf{y}_2; f) = \mathbb{E}_{\mathbf{y}_1|\mathbf{x}}\mathcal{L}_{\text{SUP}}(\mathbf{x}, \mathbf{y}_1; f) + \text{const}$, where $\hat{\mathbf{f}}(\mathbf{y}_1) \approx \mathbb{E}\{\mathbf{x}|\mathbf{y}_1\}$. However, while the minimization of \mathcal{L}_{N2N} does not require access to clean data, sampling independent pairs of noisy images $(\mathbf{y}_1, \mathbf{y}_2)$ is impractical in many real applications.

Recorrupted2Recorrupted. A more realistic scenario is the unsupervised case, with only access to unpaired noisy measurements. Assuming that the noise distribution is Gaussian $\mathbf{y} \sim \mathcal{N}(0, \mathbf{I}\sigma^2)$, R2R [7] proposed the re-corruption of noisy measurements as follows

$$\mathbf{y}_1 = \mathbf{y} + \tau\boldsymbol{\omega}, \quad \mathbf{y}_2 = \mathbf{y} - \boldsymbol{\omega}/\tau, \quad (7)$$

Model	Gaussian $\mathbf{y} \sim \mathcal{N}(\mathbf{x}, \mathbf{I}\sigma^2)$	Poisson $\mathbf{z} \sim \mathcal{P}(\mathbf{x}/\gamma), \mathbf{y} = \gamma\mathbf{z}$	Gamma $\mathbf{y} \sim \mathcal{G}(\ell, \ell/\mathbf{x})$	Binomial $\mathbf{z} \sim \text{Bin}(\ell, \mathbf{x}), \mathbf{y} = \mathbf{z}/\ell$
\mathbf{y}_1	$\mathbf{y}_1 = \mathbf{y} + \sqrt{\frac{\alpha}{1-\alpha}}\boldsymbol{\omega},$ $\boldsymbol{\omega} \sim \mathcal{N}(0, \mathbf{I}\sigma^2)$	$\mathbf{y}_1 = \frac{\mathbf{y}-\gamma\boldsymbol{\omega}}{1-\alpha},$ $\boldsymbol{\omega} \sim \text{Bin}(z, \alpha)$	$\mathbf{y}_1 = \mathbf{y} \circ (\mathbf{1} - \boldsymbol{\omega}) / (1 - \alpha),$ $\boldsymbol{\omega} \sim \text{Beta}(\ell\alpha, \ell(1 - \alpha))$	$\mathbf{y}_1 = \frac{\mathbf{y}-\boldsymbol{\omega}/\ell}{1-\alpha},$ $\boldsymbol{\omega} \sim \text{HypGeo}(\ell, \ell\alpha, \mathbf{z})$
\mathbf{y}_2	$\mathbf{y}_2 = \frac{1}{\alpha}\mathbf{y} - \frac{(1-\alpha)}{\alpha}\mathbf{y}_1$			
$\mathcal{L}_{\text{GR2R-NLL}}^\alpha$	$\ f(\mathbf{y}_1) - \mathbf{y}_2\ _2^2$	$-\gamma\mathbf{y}_2^\top \log f(\mathbf{y}_1) + \mathbf{1}^\top f(\mathbf{y}_1)$	$\log f(\mathbf{y}_1) + \mathbf{y}_2/f(\mathbf{y}_1)$	$\frac{-\mathbf{y}_2^\top \log f(\mathbf{y}_1) + (\mathbf{y}_2 - \ell)^\top \log(1 - f(\mathbf{y}_1))}{(\mathbf{y}_2 - \ell)^\top}$
$\mathcal{L}_{\text{GR2R-MSE}}^\alpha$	$\ f(\mathbf{y}_1) - \mathbf{y}_2\ _2^2$			
SURE = $\lim_{\alpha \rightarrow 0} \mathcal{L}_{\text{GR2R-MSE}}^\alpha$	$\ f(\mathbf{y}) - \mathbf{y}\ _2^2 + 2\sigma^2 \sum_{i=1}^n \frac{\partial f_i}{\partial y_i}(\mathbf{y})$	$\ f(\mathbf{y}) - \mathbf{y}\ _2^2 + 2 \sum_{i=1}^n y_i (f_i(\mathbf{y}) - f_i(\mathbf{y} - \gamma\mathbf{e}_i))$	$\ f(\mathbf{y}) - \mathbf{y}\ _2^2 + 2 \sum_{i=1}^n \sum_{k \geq 1} \frac{b(\ell, k)(-y_i)^{k+1} \Gamma(\ell)}{\Gamma(\ell+k)} \frac{\partial^k f_i}{\partial y_i^k}(\mathbf{y})$	not available ²

Table 1: **Summary of GR2R losses.** Popular noise distributions belonging to the natural exponential family and the associated splitting functions with $\alpha \in (0, 1)$, negative-log likelihood losses. As $\alpha \rightarrow 0$, the proposed GR2R loss is equivalent to a SURE-based loss, consisting of the quadratic measurement consistency and a divergence-like term. For Gamma noise $b(\ell, k) = (\ell(k-1))/(k(\ell+k-1))$.

where $\boldsymbol{\omega} \sim \mathcal{N}(\mathbf{0}, \sigma^2 \mathbf{I})$. Then, the unsupervised denoising loss is defined as

$$\mathcal{L}_{\text{R2R}}(\mathbf{y}; f) = \mathbb{E}_{\mathbf{y}_1, \mathbf{y}_2 | \mathbf{y}} \|f(\mathbf{y}_1) - \mathbf{y}_2\|_2^2. \quad (8)$$

The new measurements \mathbf{y}_1 and \mathbf{y}_2 are generated given an single \mathbf{y} . While the loss is defined with an expectation, in practice, only a single pair of $(\mathbf{y}_1, \mathbf{y}_2)$ is generated per batch of \mathbf{y} . R2R is equivalent to the supervised cost function defined in Equation (1) on the re-corruped pair \mathbf{y}_1 since $\mathbb{E}_{\mathbf{y} | \mathbf{x}} \mathcal{L}_{\text{R2R}}(\mathbf{y}; f) = \mathbb{E}_{\mathbf{y}_1 | \mathbf{x}} \mathcal{L}_{\text{SUP}}(\mathbf{x}, \mathbf{y}_1; f) + \text{const}$, where $\hat{f}(\mathbf{y}_1) \approx \mathbb{E}\{\mathbf{x} | \mathbf{y}_1\}$. Two recent works have proposed an extension of R2R to Poisson noise [21, 22] which is similar to the one presented here, while we extend these results to a much larger family of noise distributions, and show its close links with SURE.

3 Generalized R2R

We extend the R2R loss to different noise distributions. In particular, we present extensions to i) additive noise distributions beyond Gaussian noise and ii) noise distributions belonging to the natural exponential family.

3.1 Non-Gaussian Additive Noise

Assuming that $\mathbf{y} = \mathbf{x} + \boldsymbol{\epsilon}$ where the only condition is that $p(\boldsymbol{\epsilon})$ is independent of \mathbf{x} we have the following proposition.

Proposition 1. *Let $\mathbf{y} = \mathbf{x} + \boldsymbol{\epsilon}$ with noise distribution $p(\boldsymbol{\epsilon})$ independent of \mathbf{x} and let the estimator f be analytic. If \mathbf{y}_1 and \mathbf{y}_2 are sampled according to (7), then*

$$\begin{aligned} \mathcal{L}_{\text{R2R}}(\mathbf{y}; f) &\propto \mathbb{E}_{\boldsymbol{\epsilon}, \boldsymbol{\omega}} \|f(\mathbf{y} + \tau\boldsymbol{\omega}) - \mathbf{x}\|_2^2 \\ &+ \sum_{i=1}^n \sum_{k=0}^{\infty} \frac{1}{k!} \mathbb{E}_{\boldsymbol{\epsilon}_-, \boldsymbol{\omega}_-} \left\{ \frac{\partial^k f_i}{\partial x_i^k}(x_i; \mathbf{y}_- + \tau\boldsymbol{\omega}_-) \right\} \mathbb{E}_{\boldsymbol{\epsilon}_i, \boldsymbol{\omega}_i} \left(\epsilon_i - \frac{\omega_i}{\tau} \right) (\epsilon_i + \tau\omega_i)^k, \end{aligned}$$

where $\boldsymbol{\omega}$ is drawn independently of $\boldsymbol{\epsilon}$, $\mathbf{y}_- = [y_1, \dots, y_{i-1}, y_{i+1}, \dots, y_n]^\top$ and the proportionality ignores any term not including f .

The proof is included in Appendix A. In the original R2R case, $\boldsymbol{\epsilon}$ and $\boldsymbol{\omega}$ are assumed to follow the same Gaussian distribution, then $(\boldsymbol{\epsilon} - \frac{\boldsymbol{\omega}}{\tau})$ and $(\boldsymbol{\epsilon} + \tau\boldsymbol{\omega})$ are independent random variables, meaning that the error term is zero. Proposition 1 shows that the R2R loss can still be accurate beyond this assumption, showing

²In this case, $\ell \cdot \alpha$ should be a positive integer, thus the limit $\alpha \rightarrow 0$ is not available.

that low-order functions, e.g., linear reconstruction f , only require that ω matches the second-order moment ($k = 1$) of ϵ , as

$$\mathbb{E} \omega_i^2 = \mathbb{E} \epsilon_i^2, \quad (9)$$

for $i = 1, \dots, n$, whereas for quadratic functions, the case $k = 2$ imposes the constraint

$$\mathbb{E} \omega_i^3 = \frac{1}{\tau} \mathbb{E} \epsilon_i^3, \quad (10)$$

higher-order functions will require matching higher-order moments $k > 2$.

3.2 Beyond Additive Noise: Exponential family

In many applications, the noise affecting the measurements is not additive. For example, Poisson noise arises in photon-counting devices [23], and the Gamma distribution is used to model speckle noise [24]. Our main theorem extends the R2R framework to a much larger family of noise distributions, the NEF. Specifically, we assume that we obtain a measurement $\mathbf{y} \sim p(\mathbf{y}|\mathbf{x})$ where the observation model belongs to the NEF whose density is described as

$$p(\mathbf{y}|\mathbf{x}) = h(\mathbf{y}) \exp(\mathbf{y}^\top \boldsymbol{\eta}(\mathbf{x}) - \phi(\mathbf{x})), \quad (11)$$

where h , $\boldsymbol{\eta}$ and ϕ are known function according to the specific distribution (see Appendix B for examples). Among the NEF are the popular Gaussian, Poisson, Gamma, Binomial, and Beta noise distributions. For this family of measurements distribution, we generalize the corruption strategy as

$$\mathbf{y}_1 \sim p(\mathbf{y}_1|\mathbf{y}, \alpha), \quad (12)$$

$$\mathbf{y}_2 = \frac{1}{\alpha} \mathbf{y} - \frac{(1-\alpha)}{\alpha} \mathbf{y}_1, \quad (13)$$

where $p(\mathbf{y}_1|\mathbf{y}, \alpha)$ is the conditional distribution of \mathbf{y}_1 given \mathbf{y} , then, we generalize the MSE loss as

$$\mathcal{L}_{\text{GR2R-MSE}}^\alpha(\mathbf{y}; f) = \mathbb{E}_{\mathbf{y}_1, \mathbf{y}_2|\mathbf{y}, \alpha} \|f(\mathbf{y}_1) - \mathbf{y}_2\|_2^2. \quad (14)$$

According to the noise distribution of \mathbf{y} , we propose obtaining \mathbf{y}_1 and \mathbf{y}_2 in different ways, as seen in Table 1.

If the noise is Gaussian, we have that $p(\mathbf{y}_1|\mathbf{y}, \alpha) = \mathcal{N}(\mathbf{y}, \frac{\alpha \mathbf{I}}{1-\alpha})$, and the proposed loss boils down to the standard R2R loss in Eq. (7) under the change of variables $\tau = \sqrt{\frac{\alpha}{1-\alpha}}$. The following theorem demonstrated that if the pair images are generated according to Table 1, the proposed GR2R strategy is equivalent to the supervised loss.

Theorem 1. *Let $p(\mathbf{y}|\mathbf{x})$ density function of \mathbf{y} that belong to the NEF (up to a transformation of \mathbf{x}); with $\mathbb{E}\{\mathbf{y}|\mathbf{x}\} = \mathbf{x}$. The measurements admit the decomposition $\mathbf{y} = (1-\alpha)\mathbf{y}_1 + \alpha\mathbf{y}_2$ with $\alpha \in [0, 1]$ where \mathbf{y}_1 and \mathbf{y}_2 are independent random variables, generated according to Table 1, whose distribution $p_1(\mathbf{y}_1|\mathbf{x})$ and $p_2(\mathbf{y}_2|\mathbf{x})$ also belong to the NEF, with means $\mathbb{E}\{\mathbf{y}_1|\mathbf{x}\} = \mathbb{E}\{\mathbf{y}_2|\mathbf{x}\} = \mathbf{x}$, and variances $\mathbb{V}\{\mathbf{y}_1|\mathbf{x}\} = \frac{\mathbb{V}\{\mathbf{y}|\mathbf{x}\}}{1-\alpha}$ and $\mathbb{V}\{\mathbf{y}_2|\mathbf{x}\} = \frac{\mathbb{V}\{\mathbf{y}|\mathbf{x}\}}{\alpha}$. Moreover, the conditional distributions $p(\mathbf{y}_1|\mathbf{y})$ and $p(\mathbf{y}_2|\mathbf{y})$ do not depend on \mathbf{x} , we have that*

$$\mathbb{E}_{\mathbf{y}|\mathbf{x}} \mathcal{L}_{\text{GR2R-MSE}}^\alpha(\mathbf{y}; f) = \mathbb{E}_{\mathbf{y}_1|\mathbf{x}} \|f(\mathbf{y}_1) - \mathbf{x}\|_2^2.$$

The proof is included in Appendix A. One important aspect is the parameter α , consequently, by defining the signal-to-noise ratio (SNR) of a random variable \mathbf{z} as $\text{SNR}(\mathbf{z}) := \frac{\|\mathbb{E} \mathbf{z}\|_2^2}{\mathbb{E} \|\mathbf{z} - \mathbb{E} \mathbf{z}\|_2^2}$ we have that the SNR of the new variables is

$$\begin{aligned} \text{SNR}(\mathbf{y}_1) &= (1-\alpha) \text{SNR}(\mathbf{y}), \\ \text{SNR}(\mathbf{y}_2) &= \alpha \text{SNR}(\mathbf{y}), \end{aligned}$$

and thus have a strictly lower SNR than the original measurement \mathbf{y} . A good choice of α should strike the right balance between having inputs \mathbf{y}_1 with SNR close to that of \mathbf{y} , without having too noisy outputs \mathbf{y}_2 . In Appendix C, we evaluate different values of α in different noise settings, finding in most cases that the best α lies in the interval $[0.1, 0.2]$.

Equivalence with SURE Loss. Interestingly, our GR2R using MSE unsupervised loss is a generalization of the SURE loss when $\alpha \rightarrow 0$ without the need to calculate the divergence term. To show that, let us introduce the following proposition.

Proposition 2. *Assume that f is analytic, $p(\mathbf{y}|\mathbf{x})$ belongs to the NEF, and that $a_k : \mathbb{R} \mapsto \mathbb{R}$ as*

$$a_k(y_i) = \lim_{\alpha \rightarrow 0} \mathbb{E}_{y_{2,i}|y_i, \alpha} (y_{2,i} - y_i) (\alpha y_{2,i})^k,$$

for all $i = 1, \dots, n$ verifies $|a_k(y_i)| < \infty$ for all positive integers $k \geq 1$. Then,

$$\begin{aligned} \lim_{\alpha \rightarrow 0} \mathcal{L}_{\text{GR2R-MSE}}^\alpha(\mathbf{y}; f) = \\ \|f(\mathbf{y}) - \mathbf{y}\|_2^2 + 2 \sum_{i=1}^n \sum_{k \geq 1} (-1)^{k+1} a_k(y_i) \frac{1}{k!} \frac{\partial^k f_i}{\partial y_i^k}(\mathbf{y}) + \text{const.} \end{aligned}$$

The proof is included in Appendix A. With these results, Table 1 shows the equivalence for various popular noise distributions belonging to the natural exponential family. Interesting, the standard Gaussian case, we have $a_1(y_i) = \sigma^2$ and $a_k(y_i) = 0$ for $k \geq 2$, recovering the standard SURE formula. In general, if the estimator verifies $\frac{\partial^k f_i}{\partial y_i^k}(\mathbf{y}) \approx 0$ for higher order derivatives $k \geq 2$, we have

$$\begin{aligned} \lim_{\alpha \rightarrow 0} \mathcal{L}_{\text{GR2R-MSE}}^\alpha(\mathbf{y}; f) \approx \\ \|f(\mathbf{y}) - \mathbf{y}\|_2^2 + 2 \sum_{i=1}^n a_1(y_i) \frac{\partial f_i}{\partial y_i}(\mathbf{y}) + \text{const,} \end{aligned}$$

where $a_1(y_i) = \lim_{\alpha \rightarrow 0} \mathbb{V}\{y_{2,i}|y_i, \alpha\}$.

Connection with GSURE. The popular GSURE loss introduced by Eldar [18] is defined as

$$\mathcal{L}_{\text{GSURE}}(\mathbf{y}; f) = \|f(\mathbf{y}) + \nabla \log h(\mathbf{y})\|_2^2 + 2 \sum_{i=1}^n \frac{\partial f_i}{\partial y_i}(\mathbf{y}),$$

and is an unbiased estimator of

$$\mathbb{E}_{\mathbf{y}|\mathbf{x}} \mathcal{L}_{\text{GSURE}}(\mathbf{y}; f) = \mathbb{E}_{\mathbf{y}|\mathbf{x}} \|f(\mathbf{y}) - \eta(\mathbf{x})\|_2^2, \quad (15)$$

where η and h are the functions associated with the exponential family decomposition in Eq. (11). The equivalence of our method compared with GSURE only occurs for the Gaussian noise case (up to scaling of $f(\mathbf{y})$ by σ^2), where $h(\mathbf{y}) = -\sigma^2 \mathbf{y}$ and $\eta(\mathbf{x}) = \sigma^2 \mathbf{x}$. The GSURE loss targets the estimator $\hat{f}(\mathbf{y}) \approx \mathbb{E}\{\eta(\mathbf{x})|\mathbf{y}\}$, whereas in this work we focus on the conditional mean³ $\hat{f}(\mathbf{y}) \approx \mathbb{E}\{\mathbf{x}|\mathbf{y}\}$.

3.3 Negative-Log Likelihood Loss

If \mathbf{y}_1 and \mathbf{y}_2 are independent, we could use the MSE unsupervised loss, as is detailed in the previous section, as an unbiased estimator of the supervised loss $\mathcal{L}_{\text{SUP}}(\mathbf{x}, \mathbf{y}_1; f)$. Although the choice of \mathbf{y}_1 and \mathbf{y}_2 are based on the noise distribution \mathbf{y} , the MSE loss is suboptimal since it does not try to maximize the probability likelihood of the \mathbf{y} noise distribution. We propose instead to minimize the negative log-likelihood (NLL) as the loss function

$$\begin{aligned} \mathcal{L}_{\text{GR2R-NLL}}^\alpha(\mathbf{y}; f) &= \mathbb{E}_{\mathbf{y}_1, \mathbf{y}_2|\mathbf{y}} \{\phi(f(\mathbf{y}_1)) - \mathbf{y}_2^\top \eta(f(\mathbf{y}_1))\} \\ &= \mathbb{E}_{\mathbf{y}_1, \mathbf{y}_2|\mathbf{y}} \{-\log p_2(\mathbf{y}_2|\hat{\mathbf{x}} = f(\mathbf{y}_1))\} + \text{const,} \end{aligned}$$

where p_2 corresponds to the distribution of \mathbf{y}_2 given \mathbf{x} , which belongs to the exponential family, as shown in Theorem 1. For the additive Gaussian noise case, the negative log-likelihood function reduces to the standard MSE, i.e., $-\log p_2(\mathbf{y}_2|f(\mathbf{y}_1)) \propto \|f(\mathbf{y}_1) - \mathbf{y}_2\|_2^2$. Table 1 shows the losses for popular noise distributions belonging to the NEF. This loss is an unbiased estimator of a supervised negative-log-likelihood loss, whose optimal solution is also the condition mean (the proof is included in Appendix A).

³Note that in general $\eta^{-1}(\mathbb{E}\{\eta(\mathbf{x})|\mathbf{y}\}) \neq \mathbb{E}\{\mathbf{x}|\mathbf{y}\}$ for an invertible η , except for the case of linear η .

Proposition 3. *Under the assumptions of Theorem 1, we have that*

$$\mathbb{E}_{\mathbf{y}|\mathbf{x}} \mathcal{L}_{\text{GR2R-NLL}}^\alpha(\mathbf{y}; f) = \mathbb{E}_{\mathbf{y}_1|\mathbf{x}} \{-\log p_2(\mathbf{x}|f(\mathbf{y}_1))\} + \text{const},$$

whose minimizer is the minimum mean squared error estimator $f(\mathbf{y}_1) = \mathbb{E}\{\mathbf{x}|\mathbf{y}_1\}$.

3.4 Test Time Inference

Once the deep denoiser \hat{f} is trained in a self-supervised way, the following Monte Carlo approximation is used to mitigate the effect of re-corruption

$$\hat{\mathbf{x}} \approx \frac{1}{J} \sum_{j=1}^J \hat{f}(\mathbf{y}_1^{(j)}). \tag{16}$$

where $\mathbf{y}_1^{(j)} \sim p(\mathbf{y}_1|\mathbf{y}, \alpha)$ are i.i.d. samples.

4 Simulations and Results

In this section, we extend the experimental validation of the GR2R framework to denoising tasks beyond the additive Gaussian noise model, specifically addressing log-Rayleigh, Poisson and Gamma noise. We conduct a comparative analysis with state-of-the-art unsupervised denoising methods, including SURE [14], PURE [13], Neigh2Neigh [20], and Noise2Score [25], to benchmark the performance of GR2R against unbiased estimators, as well as Noise2X paradigms. To further strengthen our analysis, we replicate the original R2R framework’s reported performance on Gaussian noise. GR2R is agnostic to the choice of architecture; therefore, the DRUnet [26] architecture was utilized for Poisson denoising, while DnCNN [27] was used for denoising under the Gamma and Gaussian noise model. The code implementation was developed using the DeepInverse [28] library and is available as open source.

4.1 Non-Gaussian Additive Noise

We first evaluate the robustness of the GR2R for non-Gaussian additive noise using the DIV2K dataset with crops of 512×512 pixel resolution, with the train split (900 images) for training and the validation split (100 images) for testing. The dataset was corrupted with log-Rayleigh noise [29], which is non-symmetric, normalized to have a standard deviation $\sigma = 0.1$ and zero mean. We compare with the standard R2R [7] approach, which recorrups the noisy data using Gaussian additive noise until matching the second order moment, the noise variance, i.e., $\boldsymbol{\omega} \sim \mathcal{N}(\mathbf{0}, \mathbf{I}\sigma^2)$. We train for 100 epochs with a batch size of 16 and an initial learning rate of $5e-4$. In our GR2R approach, we generate additional noise $\boldsymbol{\omega}$ following Proposition 1 by sampling using a maximum entropy approach such that the second and third order moments conditions in Eq. (9) and Eq. (10) hold. Precisely, $\boldsymbol{\omega}$ is adjusted to match until the third order moment using a gradient descent algorithm, as presented by the authors in [30]. We computed $J = 15$ Monte Carlo Samples for the inference according to Eq. (16) for both scenarios.

The results are shown in Section 4.1. Adding the third-order correction significantly improves more than 3 dB compared with the baseline R2R, being only 0.5 dB below the supervised learning setting, with a similar variance of ± 1.51 among estimations. The reader is referred to Appendix C for additional information on the sampling algorithm.

Table 2: Mean and Variance of the PSNR/SSIM scores with the additive log-Rayleigh noise.

R2R [7] 2nd Moment	GR2R (ours) 3rd Moment	Supervised Learning
25.32 ± 0.79	29.47 ± 1.51	29.93 ± 1.50
0.576 ± 0.08	0.813 ± 0.04	0.831 ± 0.04

Table 3: PSNR/SSIM results on Poisson noise. GR2R-NLL stands for the proposed GR2R with Negative Log-Likelihood Loss.

Poisson Noise Noise Level (γ)	Methods				
	PURE [13]	Neigh2Neigh [20]	GR2R-NLL (ours)	GR2R-MSE (ours)	Supervised-MSE
0.01	32.69/0.919	33.37/0.929	33.90/0.935	33.92/0.935	33.96/0.933
0.1	24.37/0.631	28.27/0.827	28.30/0.827	28.35/0.827	28.39/0.827
0.5	22.98/0.623	24.90/0.651	25.07/0.716	24.69/0.698	25.32/0.727
1.0	17.94/0.469	23.56/0.653	23.69/0.658	23.49/0.646	23.85/0.668

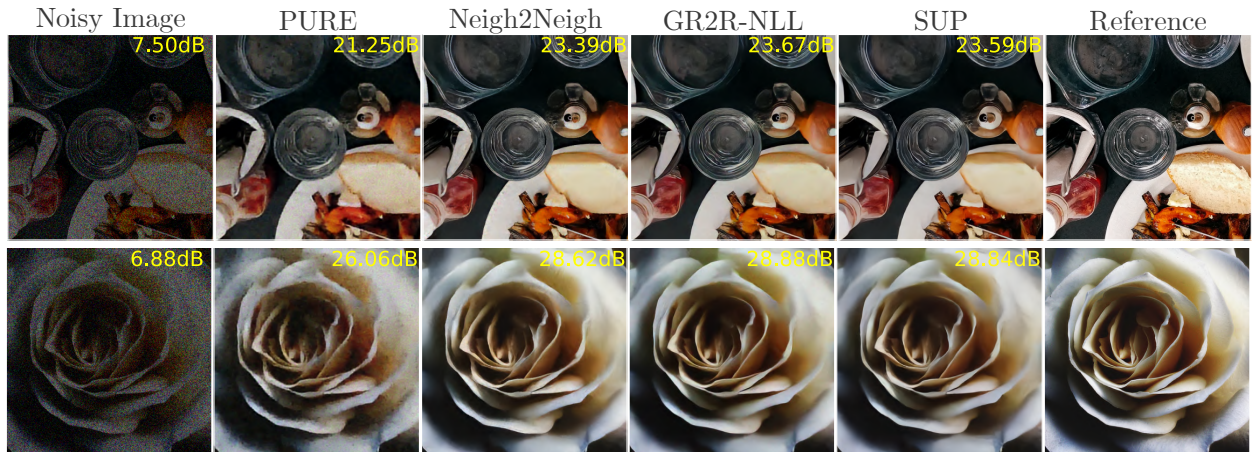


Figure 2: Denoising results for Poisson noise with $\lambda = 0.5$. The first column shows noisy input images, and the last column shows the ground truth reference. Intermediate columns present results from PURE, Neigh2Neigh, GR2R-NLL (proposed), and a supervised MSE-based method (SUP). PSNR values, shown in yellow in the top-right corner of each image, quantify the performance of each method.

4.2 Poisson Noise

We evaluate our method on the Poisson denoising problem with gain γ (as defined in Table 1) using the DIV2K dataset. The dataset, comprising high-resolution images of 512×512 resolution, was corrupted by Poisson-distributed noise. The denoising models were trained with three unsupervised approaches, including PURE and Neigh2Neigh. The training consists of 300 epochs with a batch size of 50 and an initial learning rate of $1e-3$, decreasing by a factor of 0.1 during the final 60 epochs. In our GR2R approach, training pairs were generated with a setting of $\alpha = 0.15$, as detailed in the first column of Table 1. We computed $J = 5$ Monte Carlo samples for the test according to Eq. (16).

Quantitative results for Poisson noise denoising are summarized in Table 7, with visual results presented in Figure 2. As shown, our proposed GR2R closely match the metrics of the supervised MSE-based model. GR2R-MSE performs well at higher counts (where the noise distribution is closer to Gaussian), while GR2R-NLL loss demonstrates robustness in the low-count regime. Neigh2Neigh is the second-best unsupervised technique but has drawbacks compared to GR2R. It downsamples noisy images, losing high-frequency details, and requires two model evaluations per step, increasing computational costs. GR2R, however, uses a single-term loss and one forward pass per step, making it more efficient and scalable for high-resolution image noise removal.

4.3 Gamma Noise

To examine performance under Gamma noise, we tested on the SAR Image Despeckling dataset with the number of looks $\ell \in \{1, 5, 15, 30\}$ [31]. This dataset includes 127 images with a resolution of 512×512 , each corrupted via Gamma-based sampling to simulate Gamma noise effects. Training under unsupervised methods, including Neigh2Neigh trained for 400 epochs at a batch size of 20. Starting from a learning rate of $1e-3$, the rate was decreased by a factor of 0.1 over the last 80 epochs. For the GR2R method, we generate image pairs using the parameters of the first column in Table 1, with $\alpha = 0.2$. The prediction was performed using Equation (16), where J was set to 10.

Quantitative results for Gamma noise reduction, shown in Table 8, highlight the superior performance of the GR2R framework and its GR2R-MSE variant compared to Neigh2Neigh across all tested noise levels. The supervised MSE-based method achieves the highest PSNR and SSIM, with GR2R-MSE closely matching its performance, particularly at higher SNR ($\ell = 30$). The performance between methods converges at lower SNR ($\ell = 1$); however, GR2R remains competitive with a PSNR of 32.75 dB, matching Neigh2Neigh and achieving a slightly higher SSIM. Visual comparisons in Figure 3 for Gamma noise at $\ell = 5.0$ demonstrate that GR2R and GR2R-MSE deliver enhanced image quality and reduce noise artifacts more effectively than Neigh2Neigh.

Table 4: PSNR/SSIM results on Gamma noise. GR2R-NLL stands for the proposed GR2R with Negative Log-Likelihood Loss.

Gaussian Noise	Methods			
Number of looks (ℓ)	Neigh2Neigh [20]	GR2R-NLL (ours)	GR2R-MSE (ours)	Supervised-MSE
30	30.34/0.848	30.43/0.862	31.58/0.901	31.86/0.906
15	28.56/0.802	28.71/0.824	29.55/0.862	29.76/0.865
5	25.71/0.703	25.79/0.725	26.35/0.767	26.72/0.784
1	22.19/0.560	22.19/0.545	22.38/0.599	22.56/0.611

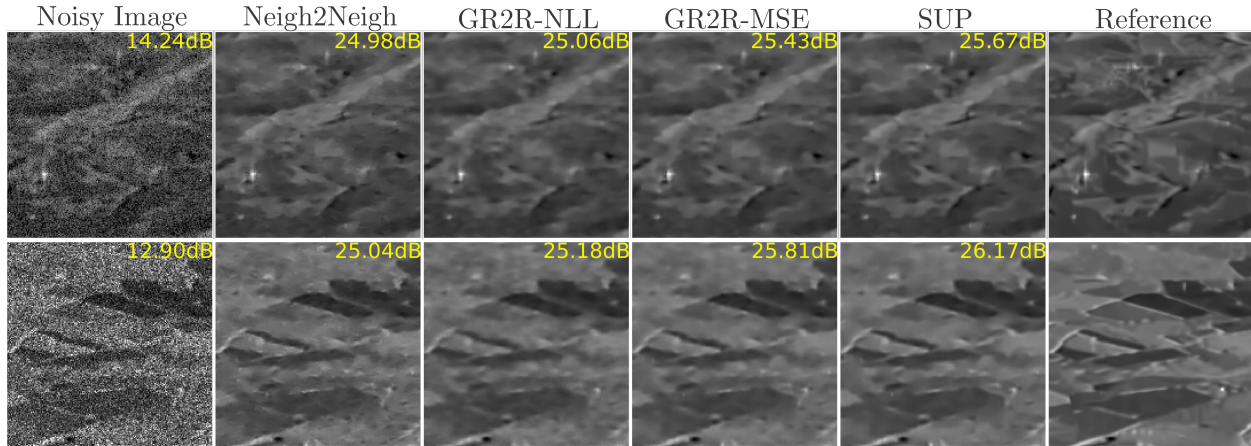


Figure 3: Denoising results for Gamma Noise with $\ell = 5$. The first column shows noisy images, and the last column shows the ground truth reference. Intermediate columns present results from Neigh2Neigh, GR2R-NLL (proposed), GR2R-MSE (proposed) and a supervised MSE-based (SUP). PSNR values, shown in yellow in the top-right corner of each image, quantify the performance of each method.

4.4 Gaussian Noise

To evaluate the performance of denoising under Gaussian noise, we tested our model on the fastMRI dataset, applying noise levels of $\sigma \in \{0.05, 0.1, 0.2, 0.5\}$. The dataset, comprising 900 images at a resolution of 256×256 , was corrupted with additive Gaussian white noise of zero mean (AGWN) at each level. Training was carried out using four unsupervised techniques: Noise2Score, SURE, Neigh2Neigh, and our proposed GR2R framework, for 600 epochs with a batch size of 32. The learning rate was initialized at 1e-3 and reduced by a factor of 0.1 over the final 48 epochs. GR2R generated training pairs in line with the configuration in the first column of Table 1, with α set to 0.5. Inference was performed using Equation (16) with $J = 5$.

Quantitative results, summarized in Table 10, show that GR2R achieves a denoising performance comparable to the supervised MSE baseline at all noise levels. This outcome is expected, given the equivalence between GR2R training and supervised training, where independent noisy image pairs are generated. Specifically, at $\sigma = 0.05$, GR2R achieves PSNR and SSIM values nearly identical to the highest performing supervised method (35.38 dB vs. 35.41 dB). At elevated noise levels, specifically $\sigma = 0.2$ and $\sigma = 0.5$, GR2R demonstrates robust denoising capabilities (30.24 dB and 25.81 dB), closely aligned with the supervised results (30.38 dB and 25.93 dB) and surpassing other self-supervised approaches.

Table 5: PSNR/SSIM results for Gaussian noise. In the case of Gaussian noise for GR2R, the MSE and NLL variants are the same.

Gaussian noise	Methods				
Noise Level (σ)	Noise2Score [25]	SURE [14]	Neigh2Neigh [20]	GR2R (ours)	Supervised-MSE
0.05	34.42/0.916	35.31/0.934	35.07/0.933	35.38/0.933	35.41/0.935
0.1	31.02/0.766	32.76/0.910	32.57/0.908	33.03/0.911	33.14/0.913
0.2	29.34/0.767	29.77/0.874	29.73/0.870	30.24/0.880	30.38/0.883
0.5	22.94/0.433	25.52/0.714	25.61/0.717	25.81/0.810	25.93/0.813

5 Extension to General Inverse Problems

The proposed method can be extended to general inverse problems $\mathbf{y} \approx \mathbf{A}\mathbf{x}$ with $\mathbf{A} \in \mathbb{R}^{m \times n}$ where the observation model $p(\mathbf{y}|\mathbf{A}\mathbf{x})$ belongs to the NEF with mean $\mathbb{E}\{\mathbf{y}|\mathbf{x}\} = \mathbf{A}\mathbf{x}$, by considering the main loss function as

$$\mathcal{L}_{\text{GR2R-MSE}}^\alpha(\mathbf{y}; f) = \mathbb{E}_{\mathbf{y}_1, \mathbf{y}_2 | \mathbf{y}} \|\mathbf{A}f(\mathbf{y}_1) - \mathbf{y}_2\|_2^2, \quad (17)$$

which is an unbiased estimator of the clean measurement consistency loss

$$\mathbb{E}_{\mathbf{x}, \mathbf{y}} \mathcal{L}_{\text{GR2R-MSE}}^\alpha(\mathbf{y}; f) = \mathbb{E}_{\mathbf{x}, \mathbf{y}_1} \|\mathbf{A}(f(\mathbf{y}_1) - \mathbf{x})\|_2^2.$$

This adaptation is straightforward from denoising to the general inverse problem in contrast to other methods, such as Neigh2Neigh, requiring that \mathbf{y} is in the image domain. If $\text{rank}(\mathbf{A}) = n$, then the GR2R minimizer is the optimal MMSE estimator, that is $\hat{f}(\mathbf{y}_1) \approx \mathbb{E}\{\mathbf{x}|\mathbf{y}_1\}$. However if $\text{rank}(\mathbf{A}) < n$, then \mathbf{A} has a non-trivial nullspace and $\hat{f}(\mathbf{y}_1) \neq \mathbb{E}\{\mathbf{x}|\mathbf{y}_1\}$. In this case, it is still possible to learn in the nullspace of \mathbf{A} if we can access a family of different $\{\mathbf{A}_g\}_{g=1}^G$ operators [32, 5] or if we can assume that the image distribution $p(\mathbf{x})$ is approximately invariant to a set of transformations $\{\mathbf{T}_g \in \mathbb{R}^{n \times n}\}_{g=1}^G$, such as translations or rotations [33, 34]. See [32] for a detailed discussion of self-supervised learning when \mathbf{A} is incomplete. These additional assumptions can be incorporated via a second loss term: in the case of a single operator \mathbf{A} and invariance, we propose to minimize

$$\mathcal{L}_{\text{GR2R-MSE}}^\alpha(\mathbf{y}; f) + \mathcal{L}_{\text{EI}}(\mathbf{y}; f) \quad (18)$$

where the Equivariant Imaging (EI) loss [33] is defined as

$$\mathcal{L}_{\text{EI}}(\mathbf{y}; f) = \mathbb{E}_g \mathbb{E}_{\mathbf{y}_1 | \mathbf{y}} \|f(\mathbf{A}\mathbf{T}_g \hat{\mathbf{x}}) - \mathbf{T}_g \hat{\mathbf{x}}\|_2^2 \quad (19)$$

with $\hat{\mathbf{x}} = f(\mathbf{y}_1)$. Figure 4 presents the results of comparing the EI framework using the \mathcal{L}_{MC} loss against EI with our GR2R strategy. We tested GR2R on the DIV2K dataset, using a binary mask A with entries

following a Bernoulli distribution with $p = 0.9$ (fixed throughout the dataset to maintain a fixed null-sapce), and corrupting measurements with Poisson noise at $\gamma = 0.05$. The results show that while EI effectively addresses the inpainting problem but still preserves the noise artifacts, in contrast, GR2R successfully tackles both denoising and inpainting simultaneously, delivering results that are comparable to its supervised counterpart. More details and experiments using other distributions are shown in AppendixC.

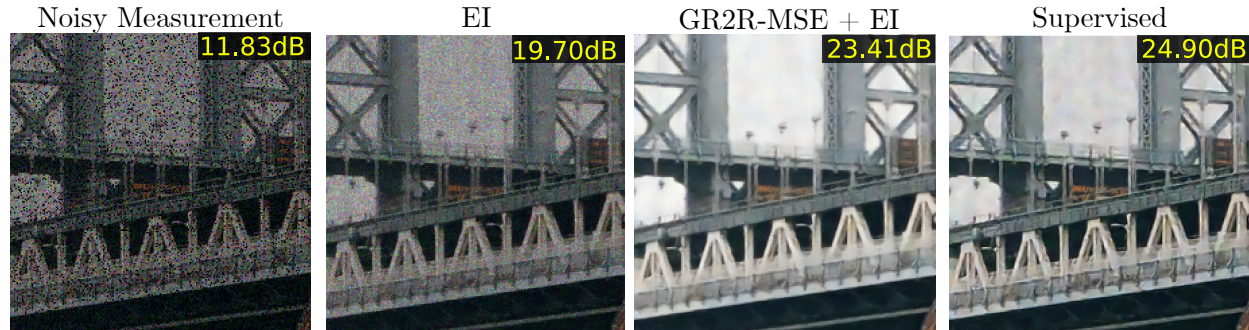


Figure 4: **GR2R on Inpainting with Poisson Noise.** We compared GR2R with the equivariant imaging framework, consisting of $\mathcal{L}_{MC} + \mathcal{L}_{EI}$, and supervised training. The the GR2R framework consists of $\mathcal{L}_{GR2R-MSE} + \mathcal{L}_{EI}$. Our findings confirm the effectiveness of GR2R for application in general inverse problems.

6 Conclusions

We present the Generalized Recorrupted-to-Recorrupted (GR2R), which extends the original R2R framework to additive noise and natural exponential family (NEF). We specifically evaluate its performance on Poisson, Gamma, and log-Rayleigh noise in addition to Gaussian noise. The key advantages are simplicity and efficiency: GR2R requires only a simple single-term loss and a single forward pass per training step, and it does not rely on continuous approximations to handle discrete noise distributions (e.g., Poisson or Binomial) used in previous methods (e.g., PURE, Noise2Score). Moreover, GR2R shows that our method recovers SURE-type loss when $\alpha \rightarrow 0$. Furthermore, our re-corruption strategy generates independent noisy pairs directly within the measurement space; naturally extends its applicability beyond image denoising to a wide range of self-supervised inverse problems as inpainting.

Acknowledgements

Julián Tachella is supported by the ANR grant UNLIP (ANR-23-CE23-0013), and VIE-UIS supports the UIS contribution under grant 3968.

References

- [1] S. Izadi, D. Sutton, and G. Hamarneh, “Image denoising in the deep learning era,” *Artificial Intelligence Review*, vol. 56, no. 7, pp. 5929–5974, 2023.
- [2] C. Belthangady and L. A. Royer, “Applications, promises, and pitfalls of deep learning for fluorescence image reconstruction,” *Nature methods*, vol. 16, no. 12, pp. 1215–1225, 2019.
- [3] G. Somepalli, V. Singla, M. Goldblum, J. Geiping, and T. Goldstein, “Diffusion art or digital forgery? investigating data replication in diffusion models,” in *Proceedings of the IEEE/CVF Conference on Computer Vision and Pattern Recognition*, 2023, pp. 6048–6058.
- [4] M. Jagielski, O. Thakkar, F. Tramer, D. Ippolito, K. Lee, N. Carlini, E. Wallace, S. Song, A. Thakurta, N. Papernot *et al.*, “Measuring forgetting of memorized training examples,” *arXiv preprint arXiv:2207.00099*, 2022.

- [5] G. Daras, K. Shah, Y. Dagan, A. Gollakota, A. Dimakis, and A. Klivans, “Ambient diffusion: Learning clean distributions from corrupted data,” *Advances in Neural Information Processing Systems*, vol. 36, 2024.
- [6] J. Lehtinen, J. Munkberg, J. Hasselgren, S. Laine, T. Karras, M. Aittala, and T. Aila, “Noise2Noise: Learning image restoration without clean data,” in *Proceedings of the 35th International Conference on Machine Learning*, ser. Proceedings of Machine Learning Research, J. Dy and A. Krause, Eds., vol. 80. PMLR, 10–15 Jul 2018, pp. 2965–2974. [Online]. Available: <https://proceedings.mlr.press/v80/lehtinen18a.html>
- [7] T. Pang, H. Zheng, Y. Quan, and H. Ji, “Recorrupted-to-recorrupted: unsupervised deep learning for image denoising,” in *Proceedings of the IEEE/CVF conference on computer vision and pattern recognition*, 2021, pp. 2043–2052.
- [8] J. Tachella, M. Davies, and L. Jacques, “Unsure: Unknown noise level stein’s unbiased risk estimator,” *arXiv preprint arXiv:2409.01985*, 2024.
- [9] A. Krull, T.-O. Buchholz, and F. Jug, “Noise2void-learning denoising from single noisy images,” in *Proceedings of the IEEE/CVF conference on computer vision and pattern recognition*, 2019, pp. 2129–2137.
- [10] J. Batson and L. Royer, “Noise2self: Blind denoising by self-supervision,” in *International Conference on Machine Learning*. PMLR, 2019, pp. 524–533.
- [11] Z. Wang, J. Liu, G. Li, and H. Han, “Blind2unblind: Self-supervised image denoising with visible blind spots,” in *Proceedings of the IEEE/CVF conference on computer vision and pattern recognition*, 2022, pp. 2027–2036.
- [12] C. M. Stein, “Estimation of the mean of a multivariate normal distribution,” *The annals of Statistics*, pp. 1135–1151, 1981.
- [13] Y. Le Montagner, E. D. Angelini, and J.-C. Olivo-Marin, “An unbiased risk estimator for image denoising in the presence of mixed poisson–gaussian noise,” *IEEE Transactions on Image processing*, vol. 23, no. 3, pp. 1255–1268, 2014.
- [14] S. Ramani, T. Blu, and M. Unser, “Monte-carlo sure: A black-box optimization of regularization parameters for general denoising algorithms,” *IEEE Transactions on image processing*, vol. 17, no. 9, pp. 1540–1554, 2008.
- [15] K. Kim, T. Kwon, and J. C. Ye, “Noise distribution adaptive self-supervised image denoising using tweedie distribution and score matching,” in *Proceedings of the IEEE/CVF Conference on Computer Vision and Pattern Recognition*, 2022, pp. 2008–2016.
- [16] N. L. Oliveira, J. Lei, and R. J. Tibshirani, “Unbiased risk estimation in the normal means problem via coupled bootstrap techniques,” *arXiv preprint arXiv:2111.09447*, 2021.
- [17] H. M. Hudson, “A natural identity for exponential families with applications in multiparameter estimation,” *The Annals of Statistics*, vol. 6, no. 3, pp. 473–484, 1978.
- [18] Y. C. Eldar, “Generalized sure for exponential families: Applications to regularization,” *IEEE Transactions on Signal Processing*, vol. 57, no. 2, pp. 471–481, 2008.
- [19] B. Yaman, S. A. H. Hosseini, S. Moeller, J. Ellermann, K. Uğurbil, and M. Akçakaya, “Self-supervised learning of physics-guided reconstruction neural networks without fully sampled reference data,” *Magnetic resonance in medicine*, vol. 84, no. 6, pp. 3172–3191, 2020.
- [20] T. Huang, S. Li, X. Jia, H. Lu, and J. Liu, “Neighbor2neighbor: Self-supervised denoising from single noisy images,” in *Proceedings of the IEEE/CVF conference on computer vision and pattern recognition*, 2021, pp. 14 781–14 790.
- [21] N. L. Oliveira, J. Lei, and R. J. Tibshirani, “Unbiased test error estimation in the poisson means problem via coupled bootstrap techniques,” *arXiv preprint arXiv:2212.01943*, 2022.
- [22] A. Krull, H. Basevi, B. Salmon, A. Zeug, F. Müller, S. Tonks, L. Muppala, and A. Leonardis, “Image denoising and the generative accumulation of photons,” in *Proceedings of the IEEE/CVF Winter Conference on Applications of Computer Vision*, 2024, pp. 1528–1537.
- [23] C. Li, X. Qu, A. Gnanasambandam, O. A. Elgendy, J. Ma, and S. H. Chan, “Photon-limited object detection using non-local feature matching and knowledge distillation,” in *Proceedings of the IEEE/CVF International Conference on Computer Vision*, 2021, pp. 3976–3987.
- [24] S. V. Parhad, K. K. Warhade, and S. S. Shitole, “Speckle noise reduction in sar images using improved filtering and supervised classification,” *Multimedia Tools and Applications*, vol. 83, no. 18, pp. 54 615–54 636, 2024.
- [25] K. Kim and J. C. Ye, “Noise2score: tweedie’s approach to self-supervised image denoising without clean images,” *Advances in Neural Information Processing Systems*, vol. 34, pp. 864–874, 2021.

- [26] K. Zhang, Y. Li, W. Zuo, L. Zhang, L. Van Gool, and R. Timofte, “Plug-and-play image restoration with deep denoiser prior,” *IEEE Transactions on Pattern Analysis and Machine Intelligence*, vol. 44, no. 10, pp. 6360–6376, 2021.
- [27] K. Zhang, W. Zuo, Y. Chen, D. Meng, and L. Zhang, “Beyond a gaussian denoiser: Residual learning of deep cnn for image denoising,” *IEEE transactions on image processing*, vol. 26, no. 7, pp. 3142–3155, 2017.
- [28] J. Tachella, D. Chen, S. Hurault, M. Terris, and A. Wang, “DeepInverse: A deep learning framework for inverse problems in imaging,” Jun. 2023. [Online]. Available: <https://github.com/deepinv/deepinv>
- [29] B. Rivet, L. Girin, and C. Jutten, “Log-rayleigh distribution: A simple and efficient statistical representation of log-spectral coefficients,” *IEEE transactions on audio, speech, and language processing*, vol. 15, no. 3, pp. 796–802, 2007.
- [30] J. Bruna and S. Mallat, “Audio texture synthesis with scattering moments,” *arXiv preprint arXiv:1311.0407*, 2013.
- [31] E. Dalsasso, X. Yang, L. Denis, F. Tupin, and W. Yang, “Sar image despeckling by deep neural networks: From a pre-trained model to an end-to-end training strategy,” *Remote Sensing*, vol. 12, no. 16, p. 2636, 2020.
- [32] J. Tachella, D. Chen, and M. Davies, “Unsupervised learning from incomplete measurements for inverse problems,” *Advances in Neural Information Processing Systems*, vol. 35, pp. 4983–4995, 2022.
- [33] D. Chen, J. Tachella, and M. E. Davies, “Equivariant imaging: Learning beyond the range space,” in *Proceedings of the IEEE/CVF International Conference on Computer Vision*, 2021, pp. 4379–4388.
- [34] —, “Robust equivariant imaging: a fully unsupervised framework for learning to image from noisy and partial measurements,” in *Proceedings of the IEEE/CVF Conference on Computer Vision and Pattern Recognition*, 2022, pp. 5647–5656.
- [35] B. Efron, *Exponential families in theory and practice*. Cambridge University Press, 2022.

A Proofs

Proof of Proposition 1

Proof. The R2R loss can be re-expressed as

$$\mathbb{E}_{\mathbf{y}_1, \mathbf{y}_2 | \mathbf{y}} \|f(\mathbf{y}_1) - \mathbf{y}_2\|_2^2 = \mathbb{E}_{\mathbf{y}_1 | \mathbf{y}} \|f(\mathbf{y}_1)\|_2^2 + \mathbb{E}_{\mathbf{y}_2 | \mathbf{y}} \|\mathbf{y}_2\|_2^2 - 2 \sum_{i=1}^n \mathbb{E}_{\mathbf{y}_1, \mathbf{y}_2, i | \mathbf{x}} y_{2,i} f_i(\mathbf{y}_1),$$

where $y_{2,i} \in \mathbb{R}$ denotes the i th entry of \mathbf{y}_2 . If the following equality

$$\mathbb{E}_{\mathbf{y}_1, \mathbf{y}_2, i | \mathbf{x}} y_{2,i} f_i(\mathbf{y}_1) = x_i \mathbb{E}_{\mathbf{y}_1 | \mathbf{x}} f_i(\mathbf{y}_1), \quad (20)$$

holds (below is how to ensure this) for all $i = 1, \dots, n$, then

$$\begin{aligned} \mathbb{E}_{\mathbf{y}_1, \mathbf{y}_2 | \mathbf{x}} \|f(\mathbf{y}_1) - \mathbf{y}_2\|_2^2 &= \mathbb{E}_{\mathbf{y}_1 | \mathbf{x}} \|f(\mathbf{y}_1)\|_2^2 + \mathbb{E}_{\mathbf{y}_2 | \mathbf{x}} \|\mathbf{y}_2\|_2^2 - 2 \sum_{i=1}^n x_i \mathbb{E}_{\mathbf{y}_1 | \mathbf{x}} f_i(\mathbf{y}_1) \\ &= \mathbb{E}_{\mathbf{y}_2 | \mathbf{x}} \|f(\mathbf{y}_1) - \mathbf{x}\|_2^2 - \|\mathbf{x}\|_2^2 + \mathbb{E}_{\mathbf{y}_2 | \mathbf{x}} \|\mathbf{y}_2\|_2^2 \\ &= \mathbb{E}_{\mathbf{y}_2 | \mathbf{x}} \|f(\mathbf{y}_1) - \mathbf{x}\|_2^2 + \text{const}, \end{aligned} \quad (21)$$

where the second line comes from adding and subtracting $\|\mathbf{x}\|_2$.

A sufficient (but not necessary) condition for (20) to hold is that i) \mathbf{y}_1 and \mathbf{y}_2 are independent and ii) $\mathbb{E}_{\mathbf{y}_2 | \mathbf{x}} \mathbf{y}_2 = \mathbf{x}$. If this conditions hold, we trivially have $\mathbb{E}_{\mathbf{y}_1, \mathbf{y}_2, i | \mathbf{x}} y_{2,i} f_i(\mathbf{y}_1) = \left(\mathbb{E}_{\mathbf{y}_2, i | \mathbf{x}} y_{2,i}\right) \left(\mathbb{E}_{\mathbf{y}_1 | \mathbf{x}} f_i(\mathbf{y}_1)\right) = x_i \mathbb{E}_{\mathbf{y}_1 | \mathbf{x}} f_i(\mathbf{y}_1)$ for $i = 1, \dots, n$. We will analyze the necessary condition (beyond independence) for the case of additive noise where $\mathbf{y} = \mathbf{x} + \boldsymbol{\epsilon}$ where $\boldsymbol{\epsilon}$ is sampled from a symmetric noise distribution that is independent across pixel entries. We construct pairs $\mathbf{y}_1 = \mathbf{y} + \boldsymbol{\omega}\tau$ and $\mathbf{y}_2 = \mathbf{y} - \boldsymbol{\omega}/\tau$, with $\tau > 0$ and $\boldsymbol{\omega}$ sampled from the same distribution as $\boldsymbol{\epsilon}$. Due to the independence across entries, we will drop the i th indices and define the scalar function $f_i(\cdot; \mathbf{y}_{1,-i}) : \mathbb{R} \mapsto \mathbb{R}$, such that the left-hand side of (20) can be simplified to

$$\mathbb{E}_{\epsilon_i, \omega_i} \underbrace{(x_i + \epsilon_i - \omega_i/\tau)}_{y_{2,i}} f_i \underbrace{(x_i + \epsilon_i + \tau\omega_i)}_{y_{1,i}}; \mathbf{y}_{1,-i} = x_i \mathbb{E}_{\epsilon_i, \omega_i} f_i(x_i + \epsilon_i + \tau\omega_i; \mathbf{y}_{1,-i}) - \mathbb{E}_{\epsilon_i, \omega_i} \left(\epsilon_i - \frac{\omega_i}{\tau}\right) f_i(x_i + \epsilon_i + \tau\omega_i; \mathbf{y}_{1,-i}), \quad (22)$$

where ω_i , x_i and ϵ_i refer to the i th entry, and are thus one-dimensional. In this additive case, showing (22) is equivalent to showing that

$$\mathbb{E}_{\epsilon_i, \omega_i} \left(\epsilon_i - \frac{\omega_i}{\tau}\right) f_i(x_i + \epsilon_i + \tau\omega_i; \mathbf{y}_{1,-i}) = 0. \quad (23)$$

Assuming that f_i is analytic (that is, is infinitely differentiable and has a convergent Taylor expansion) and performing a Taylor expansion of f_i around x_i , we obtain

$$\begin{aligned} \mathbb{E}_{\epsilon_{-i}, \omega_{-i}} \mathbb{E}_{\epsilon_i, \omega_i} \left(\epsilon_i - \frac{\omega_i}{\tau}\right) f_i(x_i + \epsilon_i + \omega_i\tau; \mathbf{y}_{1,-i}) &= \mathbb{E}_{\epsilon_{-i}, \omega_{-i}} \mathbb{E}_{\epsilon_i, \omega_i} \left(\epsilon_i - \frac{\omega_i}{\tau}\right) \sum_{k \geq 0} \frac{1}{k!} \frac{\partial^k f_i}{\partial x_i^k}(x_i; \mathbf{y}_{1,-i}) (\epsilon_i + \tau\omega_i)^k \\ &= \sum_{k \geq 0} \frac{1}{k!} \mathbb{E}_{\epsilon_{-i}, \omega_{-i}} \left\{ \frac{\partial^k f_i}{\partial x_i^k}(x_i; \mathbf{y}_{1,-i}) \right\} \mathbb{E}_{\epsilon_i, \omega_i} \left(\epsilon_i - \frac{\omega_i}{\tau}\right) (\epsilon_i + \tau\omega_i)^k \end{aligned}$$

where the case $k = 0$ is removed from the last sum as $\mathbb{E}_{\epsilon_i, \omega_i} \left\{ \epsilon_i - \frac{\omega_i}{\tau} \right\} = 0$ if the two noises have zero mean. \square

Proof of Theorem 1

Proof. If the observation model belongs to the natural exponential family (NEF), we can write it as

$$p(\mathbf{y}|\mathbf{x}) = h(\mathbf{y}) \exp(\mathbf{y}^\top \eta(\mathbf{x}) - \phi(\mathbf{x})),$$

with $\mathbf{x}, \mathbf{y} \in \mathbb{R}^n$, and $h : \mathbb{R} \mapsto \mathbb{R}$ $\eta : \mathbb{R} \mapsto \mathbb{R}$ and $\phi : \mathbb{R} \mapsto \mathbb{R}$ elementwise functions which change according to the distribution. NEF distributions verify the following properties [35]

1. η is an invertible function.
2. ϕ is strictly convex.
3. Given ϕ and η , h is given by the Laplace transform $h(\mathbf{y}) = \int \exp(-\mathbf{s}^\top \mathbf{y} + \phi(\eta^{-1}(\mathbf{s}))) d\mathbf{s}$.
4. The mean of each entry is given by

$$\mathbb{E}\{y_i|x_i\} = \frac{\partial \phi}{\partial x_i}(x_i) / \frac{\partial \eta}{\partial x_i}(x_i) = x_i, \quad (24)$$

for $i = 1, \dots, n$.

We look for the decomposition $\mathbf{y} = (1 - \alpha)\mathbf{y}_1 + \alpha\mathbf{y}_2$ such that \mathbf{y}_1 and \mathbf{y}_2 also belong to the NEF, i.e.,

$$p_1(\mathbf{y}_1|\mathbf{x}) = h_1(\mathbf{y}_1) \exp(\mathbf{y}_1^\top \eta_1(\mathbf{x}) - \phi_1(\mathbf{x})), \quad (25)$$

and

$$p_2(\mathbf{y}_2|\mathbf{x}) = h_2(\mathbf{y}_2) \exp(\mathbf{y}_2^\top \eta_2(\mathbf{x}) - \phi_2(\mathbf{x})), \quad (26)$$

for some $\alpha \in (0, 1)$. Hence, the element-by-element functions of \mathbf{y}_1 , \mathbf{y}_2 are related to those of \mathbf{y} as $\phi_1(\mathbf{x}) = (1 - \alpha)\phi(\mathbf{x})$, $\phi_2(\mathbf{x}) = \alpha\phi(\mathbf{x})$, $\eta_1(\mathbf{x}) = (1 - \alpha)\eta(\mathbf{x})$, $\eta_2(\mathbf{x}) = \alpha\eta(\mathbf{x})$, $h_1(\mathbf{y}_1) = \int \exp\left(-\mathbf{s}^\top \mathbf{y}_1 + (1 - \alpha)\phi\left(\eta^{-1}\left(\frac{\mathbf{s}}{1 - \alpha}\right)\right)\right) d\mathbf{s}$ and $h_2(\mathbf{y}_2) = \int \exp\left(-\mathbf{s}^\top \mathbf{y}_2 + \alpha\phi\left(\eta^{-1}\left(\frac{\mathbf{s}}{\alpha}\right)\right)\right) d\mathbf{s}$.

We first verify that this choice gives the right distribution for \mathbf{y} :

$$\begin{aligned} p(\mathbf{y}|\mathbf{x}) &= \int p_1(\mathbf{y}_1|\mathbf{x}) p_2\left(\frac{1}{\alpha}\mathbf{y} - \frac{1 - \alpha}{\alpha}\mathbf{y}_1|\mathbf{x}\right) d\mathbf{y}_1 \\ &= \exp(\mathbf{y}^\top \eta(\mathbf{x}) - \phi(\mathbf{x})) \int h_1(\mathbf{y}_1) h_2\left(\frac{1}{\alpha}\mathbf{y} - \frac{1 - \alpha}{\alpha}\mathbf{y}_1\right) d\mathbf{y}_1, \end{aligned}$$

where the second line uses the fact that

$$p_1(\mathbf{y}_1|\mathbf{x}) p_2\left(\frac{1}{\alpha}\mathbf{y} - \frac{1 - \alpha}{\alpha}\mathbf{y}_1|\mathbf{x}\right) = h_1(\mathbf{y}_1) \exp\left((1 - \alpha)\mathbf{y}_1^\top \eta(\mathbf{x}) - (1 - \alpha)\phi(\mathbf{x})\right) h_2\left(\frac{1}{\alpha}\mathbf{y} - \frac{1 - \alpha}{\alpha}\mathbf{y}_1\right) \times \quad (27)$$

$$\exp\left(\alpha\left(\frac{1}{\alpha}\mathbf{y} - \frac{1 - \alpha}{\alpha}\mathbf{y}_1\right)^\top \eta(\mathbf{x}) - \alpha\phi(\mathbf{x})\right) \quad (28)$$

$$= \exp(\mathbf{y}^\top \eta(\mathbf{x}) - \phi(\mathbf{x})) h_1(\mathbf{y}_1) h_2\left(\frac{1}{\alpha}\mathbf{y} - \frac{1 - \alpha}{\alpha}\mathbf{y}_1\right). \quad (29)$$

We can obtain the conditional distribution of \mathbf{y}_1 given \mathbf{y} as

$$p(\mathbf{y}_1|\mathbf{y}, \mathbf{x}) = \frac{1}{p(\mathbf{y}|\mathbf{x})} p(\mathbf{y}|\mathbf{y}_1, \mathbf{x}) p_1(\mathbf{y}_1|\mathbf{x}),$$

due to Bayes theorem. Using the fact that $p(\mathbf{y}|\mathbf{y}_1, \mathbf{x}) = p_2\left(\frac{1}{\alpha}\mathbf{y} - \frac{1 - \alpha}{\alpha}\mathbf{y}_1|\mathbf{x}\right)$ we obtain

$$\begin{aligned} p(\mathbf{y}_1|\mathbf{y}, \mathbf{x}) &= \frac{1}{p(\mathbf{y}|\mathbf{x})} p_1(\mathbf{y}_1|\mathbf{x}) p_2\left(\frac{1}{\alpha}\mathbf{y} - \frac{1 - \alpha}{\alpha}\mathbf{y}_1|\mathbf{x}\right) \\ &= \frac{h_1(\mathbf{y}_1) h_2(\mathbf{y} - \mathbf{y}_1)}{h(\mathbf{y})}, \end{aligned} \quad (30)$$

where we use again (29). Thus we have that $p(\mathbf{y}_1|\mathbf{y}, \mathbf{x})$ does not depend on the unknown parameter \mathbf{x} , that is $p(\mathbf{y}_1|\mathbf{y}, \mathbf{x}) = p(\mathbf{y}_1|\mathbf{y})$. Consequently, since \mathbf{y}_1 and \mathbf{y}_2 are independent conditional on \mathbf{x} and $\mathbb{E}_{\mathbf{y}_2|\mathbf{x}}\{\mathbf{y}_2 - \mathbf{x}\} = \mathbb{E}\{\mathbf{y}_2|\mathbf{x}\} - \mathbf{x} = \mathbf{0}$, we have that

$$\begin{aligned} \mathbb{E}_{\mathbf{y}_1, \mathbf{y}_2|\mathbf{x}} \|f(\mathbf{y}_1) - \mathbf{y}_2\|_2^2 &= \mathbb{E}_{\mathbf{y}_1|\mathbf{x}} \|f(\mathbf{y}_1) - \mathbf{x}\|_2^2 + 2\mathbb{E}_{\mathbf{y}_1, \mathbf{y}_2|\mathbf{x}} \{(f(\mathbf{y}_1) - \mathbf{x})^\top (\mathbf{x} - \mathbf{y}_2)\} + \mathbb{E}_{\mathbf{y}_2|\mathbf{x}} \|\mathbf{x} - \mathbf{y}_2\|_2^2 \\ &= \mathbb{E}_{\mathbf{y}_1|\mathbf{x}} \|f(\mathbf{y}_1) - \mathbf{x}\|_2^2 + 2\mathbb{E}_{\mathbf{y}_1|\mathbf{x}} \{f(\mathbf{y}_1)\}^\top \mathbb{E}_{\mathbf{y}_2|\mathbf{x}} \{\mathbf{y}_2 - \mathbf{x}\} - \underbrace{2\mathbb{E}_{\mathbf{y}_2|\mathbf{x}} \{\mathbf{x}^\top (\mathbf{x} - \mathbf{y}_2)\} + \mathbb{E}_{\mathbf{y}_2|\mathbf{x}} \|\mathbf{x} - \mathbf{y}_2\|_2^2}_{\text{const}} \\ &= \mathbb{E}_{\mathbf{y}_1|\mathbf{x}} \|f(\mathbf{y}_1) - \mathbf{x}\|_2^2 + \text{const}. \end{aligned}$$

□

Proof of Proposition 2

Proof. We can write the GR2R-MSE loss as

$$\mathcal{L}_{\text{GR2R-MSE}}^\alpha(\mathbf{y}; f) = \mathbb{E}_{\mathbf{y}_2|\mathbf{y}} \|f(\frac{\mathbf{y} - \mathbf{y}_2^\alpha}{1 - \alpha}) - \mathbf{y}_2\|_2^2 \quad (31)$$

$$= \mathbb{E}_{\mathbf{y}_2|\mathbf{y}} \|f(\frac{\mathbf{y} - \mathbf{y}_2^\alpha}{1 - \alpha}) - \mathbf{y} - (\mathbf{y}_2 - \mathbf{y})\|_2^2 \quad (32)$$

$$= \mathbb{E}_{\mathbf{y}_2|\mathbf{y}} \|f(\frac{\mathbf{y} - \mathbf{y}_2^\alpha}{1 - \alpha}) - \mathbf{y}\|_2^2 - \mathbb{E}_{\mathbf{y}_2|\mathbf{y}} 2 \sum_{i=1}^n (y_{2,i} - y_i) f_i(\frac{\mathbf{y} - \mathbf{y}_2^\alpha}{1 - \alpha}) + \text{const}. \quad (33)$$

Since by assumption f is analytic, we can apply a Taylor expansion to the second term, i.e., $f_i(\frac{\mathbf{y} - \mathbf{y}_2^\alpha}{1 - \alpha}) = \sum_{k \geq 0} \frac{1}{k!} \frac{\partial^k f_i}{\partial y_i^k}(\frac{\mathbf{y} - \mathbf{y}_{2,-i}^\alpha}{1 - \alpha}) \frac{(-1)^k \alpha^k}{(1 - \alpha)^k} y_{i,2}^k$, where $\mathbf{y}_{2,-i} \in \mathbb{R}^n$ has the i th entry equal to zero and the rest equal to \mathbf{y}_2 . Thus we obtain:

$$\mathcal{L}_{\text{GR2R-MSE}}^\alpha(\mathbf{y}; f) \propto \mathbb{E}_{\mathbf{y}_2|\mathbf{y}} \left(\|f(\frac{\mathbf{y} - \mathbf{y}_2^\alpha}{1 - \alpha}) - \mathbf{y}\|_2^2 - 2 \sum_{i=1}^n \sum_{k \geq 1} \frac{1}{k!} \frac{\partial^k f_i}{\partial y_i^k}(\frac{\mathbf{y} - \mathbf{y}_{2,-i}^\alpha}{1 - \alpha}) \frac{(-1)^k}{(1 - \alpha)^k} (y_{2,i} - y_i) (\alpha y_{2,i})^k \right),$$

where we used the fact that for $k = 0$ we have $\mathbb{E}\{y_{2,i} - y_i | y_i\} = 0$. Taking the limit $\alpha \rightarrow 0$, we obtain⁴

$$\begin{aligned} \lim_{\alpha \rightarrow 0} \mathcal{L}_{\text{GR2R-MSE}}^\alpha(\mathbf{y}; f) &\propto \lim_{\alpha \rightarrow 0} \mathbb{E}_{\mathbf{y}_2|\mathbf{y}} \|f(\frac{\mathbf{y} - \mathbf{y}_2^\alpha}{1 - \alpha}) - \mathbf{y}\|_2^2 \\ &\quad - 2 \sum_{i=1}^n \sum_{k \geq 1} \frac{1}{k!} \mathbb{E}_{\mathbf{y}_{2,-i}|\mathbf{y}} \left\{ \frac{\partial^k f_i}{\partial y_i^k}(\frac{\mathbf{y} - \mathbf{y}_{2,-i}^\alpha}{1 - \alpha}) \right\} \frac{(-1)^k}{(1 - \alpha)^k} \mathbb{E}_{\mathbf{y}_{2,i}|y_i} (y_{2,i} - y_i) (\alpha y_{2,i})^k \\ &\propto \|f(\mathbf{y}) - \mathbf{y}\|_2^2 + 2 \sum_{i=1}^n \sum_{k \geq 1} (-1)^{k+1} \frac{1}{k!} \frac{\partial^k f_i}{\partial y_i^k}(\mathbf{y}) \lim_{\alpha \rightarrow 0} \mathbb{E}\{(y_{2,i} - y_i) (\alpha y_{2,i})^k | y_i, \alpha\} \end{aligned}$$

where the last line uses the fact that $a_k(y_i) = \lim_{\alpha \rightarrow 0} \mathbb{E}_{\mathbf{y}_{2,i}|y_i, \alpha} \{(y_{2,i} - y_i) (\alpha y_{2,i})^k\}$ converges for all positive integer k . Replacing the definition of a_k in the previous formula, we obtain the desired result:

$$\lim_{\alpha \rightarrow 0} \mathcal{L}_{\text{GR2R-MSE}}^\alpha(\mathbf{y}; f) \propto \|f(\mathbf{y}) - \mathbf{y}\|_2^2 + 2 \sum_{i=1}^n \sum_{k \geq 1} (-1)^{k+1} a_k(y_i) \frac{1}{k!} \frac{\partial^k f_i}{\partial y_i^k}(\mathbf{y}).$$

□

⁴We have that for $g: \mathbb{R}^n \mapsto \mathbb{R}$, the expectation $\mathbb{E}_{\mathbf{y}_2|\mathbf{y}} g(\alpha \mathbf{y}_2) = g(\mathbf{0})$ as $p(\alpha \mathbf{y}_2|\mathbf{y}) \rightarrow \delta_{\mathbf{y}_2=\mathbf{0}}$ as $\alpha \rightarrow 0$.

Proof of Proposition 3

Proof. The $\mathcal{L}_{\text{GR2R}}^\alpha(\mathbf{y}; f)$ is defined as

$$\begin{aligned}
\mathbb{E}_{\mathbf{y}_1, \mathbf{y}_2 | \mathbf{x}} - \log p_2(\mathbf{y}_2 | \hat{\mathbf{x}} = f(\mathbf{y}_1)) &= \mathbb{E}_{\mathbf{y}_1, \mathbf{y}_2 | \mathbf{x}} \{ -\alpha \mathbf{y}_2^\top \eta(f(\mathbf{y}_1)) + \alpha \phi(f(\mathbf{y}_1)) - \log h_2(\mathbf{y}_2) \} \\
&= -\alpha (\mathbb{E}_{\mathbf{y}_2 | \mathbf{x}} \mathbf{y}_2^\top) \mathbb{E}_{\mathbf{y}_1 | \mathbf{x}} \eta(f(\mathbf{y}_1)) + \mathbb{E}_{\mathbf{y}_1 | \mathbf{x}} \alpha \phi(f(\mathbf{y}_1)) - \mathbb{E}_{\mathbf{y}_2 | \mathbf{x}} \log h_2(\mathbf{y}_2) \\
&= -\alpha \mathbf{x}^\top \mathbb{E}_{\mathbf{y}_1 | \mathbf{x}} \eta(f(\mathbf{y}_1)) + \mathbb{E}_{\mathbf{y}_1 | \mathbf{x}} \alpha \phi(f(\mathbf{y}_1)) - \mathbb{E}_{\mathbf{y}_2 | \mathbf{x}} \log h_2(\mathbf{y}_2) \\
&= -\mathbb{E}_{\mathbf{y}_1 | \mathbf{x}} \{ \alpha \mathbf{x}^\top \eta(f(\mathbf{y}_1)) - \alpha \phi(f(\mathbf{y}_1)) + \log h_2(\mathbf{y}_2) \} + \text{const} \\
&= \mathbb{E}_{\mathbf{y}_1 | \mathbf{x}} - \log p_2(\mathbf{x} | \hat{\mathbf{x}} = f(\mathbf{y}_1)) + \text{const}.
\end{aligned} \tag{34}$$

We now prove that $\mathbb{E}\{\mathbf{x} | \mathbf{y}_1\} = \arg \min_f \mathcal{L}_{\text{GR2R}}^\alpha(\mathbf{y}; f)$. We can write this minimization as

$$\min_f \mathbb{E}_{\mathbf{x}, \mathbf{y}_1} \{ \eta(f(\mathbf{y}_1))^\top \mathbf{x} - \phi(f(\mathbf{y}_1)) \} = \min_f \mathbb{E}_{\mathbf{y}_1} \{ \eta(f(\mathbf{y}_1))^\top \mathbb{E}\{\mathbf{x} | \mathbf{y}_1\} - \phi(f(\mathbf{y}_1)) \} \tag{35}$$

$$= \mathbb{E}_{\mathbf{y}_1} \{ \min_f \eta(f(\mathbf{y}_1))^\top \mathbb{E}\{\mathbf{x} | \mathbf{y}_1\} - \phi(f(\mathbf{y}_1)) \}, \tag{36}$$

where the last equality swaps the integration with the minimization since the minimizer exists for every fixed \mathbf{y}_1 . Defining $\mathbf{z} := f(\mathbf{y}_1)$, we can minimize the term inside the expectation w.r.t. to

$$\arg \min_{\mathbf{z}} \mathbb{E}\{\mathbf{x} | \mathbf{y}_1\} \eta(\mathbf{z}) - \phi(\mathbf{z}). \tag{37}$$

The problem is separable across entries, so it can be

$$\arg \min_{z_i} \mathbb{E}\{x_i | y_{1,i}\} \eta(z_i) - \phi(z_i), \tag{38}$$

for $i = 1, \dots, n$. Since the problem is strongly convex w.r.t. z_i , we can find the solution by setting its derivative to zero

$$\mathbb{E}\{x_i | y_{1,i}\} \frac{\partial \eta}{\partial z_i}(\hat{z}_i) - \frac{\partial \phi}{\partial z_i}(\hat{z}_i) = 0 \tag{39}$$

$$\frac{\partial \eta}{\partial z_i}(\hat{z}_i) / \frac{\partial \phi}{\partial z_i}(\hat{z}_i) = \mathbb{E}\{x_i | y_{1,i}\} \tag{40}$$

$$\hat{z}_i = \mathbb{E}\{x_i | y_{1,i}\}, \tag{41}$$

for $i = 1, \dots, n$, where the second line uses property (24), and thus $\hat{f}(\mathbf{y}_1) = \mathbb{E}\{\mathbf{x} | \mathbf{y}_1\}$. □

B Additional information

Table 6 summarizes the NEF distributions $p(\mathbf{y} | \mathbf{x})$ used in the main document. This was used to create the recorruptions used in the main document. Specifically, the formulas to construct \mathbf{y}_1 in terms of \mathbf{y} and the extra noise $\boldsymbol{\omega}$ can be derived from replacing $h(y)$, $h_1(y_1)$ and $h_2(y_2)$ from Table 6 in Equation (30) for its respective NEF distribution; this is left as an exercise for the reader.

Model	$y \sim \mathcal{N}(x, \sigma^2)$	$y \sim \mathcal{P}(\frac{x}{\gamma})$	$y \sim \mathcal{G}(\ell, x/\ell)$	$y \sim \text{Bin}(\ell, x)$
$\eta(x)$	x/σ^2	$\log(x)$	$-\ell/x$	$\log(x/(1-x))$
$\phi(x)$	$x^2/(2\sigma^2)$	x/γ	$\ell \log(x)$	$\ell \log(1-x)$
$h(y)$	$\sqrt{2\pi}\sigma \exp(y^2/(2\sigma^2))$	$(\gamma^y y!)^{-1}$	$\ell^\ell y^{\ell-1}/\Gamma(\ell)$	$\binom{\ell}{y}$
$h_1(y_1)$	$\sqrt{2\pi} \frac{\sigma}{\sqrt{1-\alpha}} \exp(y_1^2/(2\frac{\sigma^2}{1-\alpha}))$	$((1-\alpha)^{(1-\alpha)y_1+1} \gamma^{(1-\alpha)y_1} ((1-\alpha)y_1!)^{-1})$	$\frac{\ell^{(1-\alpha)\ell} ((1-\alpha)y_1)^{(1-\alpha)\ell-1}}{(1-\alpha)\Gamma((1-\alpha)\ell)}$	$\frac{1}{1-\alpha} \binom{(1-\alpha)\ell}{(1-\alpha)y_1}$
$h_2(y_2)$	$\sqrt{2\pi} \frac{\sigma}{\sqrt{\alpha}} \exp(y_2^2/(2\frac{\sigma^2}{\alpha}))$	$(\alpha^{\alpha y_2+1} \gamma^{\alpha y_2} (\alpha y_2!)^{-1})$	$\frac{\ell^{\alpha\ell} (\alpha y_2)^{\alpha\ell-1}}{\alpha\Gamma(\alpha\ell)}$	$\frac{1}{\alpha} \binom{\alpha\ell}{\alpha y_2}$

Table 6: Examples of one-dimensional natural exponential family distributions $p(y|x)$ and their respective decompositions. These can be extended to higher dimensions by considering separable distributions $p(\mathbf{y}|\mathbf{x}) = \prod_{i=1}^n p(y_i|x_i)$, by $\eta(\mathbf{x}) = \sum_{i=1}^n \eta(x_i)$, $\phi(\mathbf{x}) = \sum_{i=1}^n \phi(x_i)$, $h(\mathbf{y}) = \prod_{i=1}^n h(y_i)$, $h_1(\mathbf{y}_1) = \prod_{i=1}^n h_1(y_{1,i})$ and $h_2(\mathbf{y}_2) = \prod_{i=1}^n h_2(y_{2,i})$.

Equivalence with SURE as $\alpha \rightarrow 0$

$$\lim_{\alpha \rightarrow 0} \mathcal{L}_{\text{GR2R-MSE}}^\alpha(\mathbf{y}; f) = \|\mathbf{f}(\mathbf{y}) - \mathbf{y}\|_2^2 + 2 \sum_{i=1}^n \sum_{k \geq 1} (-1)^{k+1} a_k(y_i) \frac{1}{k!} \frac{\partial^k f_i}{\partial y_i^k}(\mathbf{y}) + \text{const.} \quad (42)$$

where

$$a_k(y_i) = \lim_{\alpha \rightarrow 0} \mathbb{E}_{y_{2,i}|y_i,\alpha} (y_{2,i} - y_i) (\alpha y_{2,i})^k. \quad (43)$$

Gaussian case. Based on the proposed re-corraption procedure for the Gaussian case, we have that the re-corraption of \mathbf{y}_2 in terms of \mathbf{y} and the extra noise $\boldsymbol{\omega}$ as

$$\mathbf{y}_2 = \mathbf{y} - \sqrt{\frac{1-\alpha}{\alpha}} \boldsymbol{\omega} \quad (44)$$

Analyze for $k = 1$

$$a_1(y_i) = \lim_{\alpha \rightarrow 0} \mathbb{E}_{y_{2,i}|y_i,\alpha} \{(y_{2,i} - y_i) (\alpha y_{2,i})^1\} \quad (45)$$

for one element y_2, y

$$\begin{aligned} \lim_{\alpha \rightarrow 0} \mathbb{E}_{y_2|y,\alpha} \{(y_2 - y) (\alpha y_2)\} &= \lim_{\alpha \rightarrow 0} \mathbb{E}_{\omega|y,\alpha} \{\alpha(y - \sqrt{\frac{1-\alpha}{\alpha}} \omega - y)(y - \sqrt{\frac{1-\alpha}{\alpha}} \omega)\} \\ &= \lim_{\alpha \rightarrow 0} \mathbb{E}_{\omega|y,\alpha} \{-\alpha \sqrt{\frac{1-\alpha}{\alpha}} \omega (y - \sqrt{\frac{1-\alpha}{\alpha}} \omega)\} \\ &= \lim_{\alpha \rightarrow 0} \mathbb{E}_{\omega|y,\alpha} \{-\alpha \sqrt{\frac{1-\alpha}{\alpha}} \omega y + \alpha \frac{1-\alpha}{\alpha} \omega^2\} \\ &= \lim_{\alpha \rightarrow 0} \mathbb{E}_{\omega|y,\alpha} \{-\sqrt{\alpha(1-\alpha)} \omega y + (1-\alpha) \omega^2\} \\ &= \lim_{\alpha \rightarrow 0} (1-\alpha) \sigma^2 = \sigma^2 \end{aligned} \quad (46)$$

analyzing for $k > 1$ we have that $a_k(y) \rightarrow 0$ since the α^{k-1} term dominates in the expression

$$a_k(y) = \lim_{\alpha \rightarrow 0} \mathbb{E}_{\omega|y,\alpha} \left\{ (-\sqrt{\alpha(1-\alpha)} \omega y + (1-\alpha) \omega^2) (y - \sqrt{\frac{1-\alpha}{\alpha}} \omega)^{k-1} \alpha^{k-1} \right\} \quad (47)$$

finally, substituting $a_k(y_i)$ in (42) for the Gaussian case we have that

$$\lim_{\alpha \rightarrow 0} \mathcal{L}_{\text{GR2R-MSE}}^\alpha(\mathbf{y}; f) = \|\mathbf{f}(\mathbf{y}) - \mathbf{y}\|_2^2 + 2\sigma^2 \sum_{i=1}^n \frac{\partial^k f_i}{\partial y_i^k}(\mathbf{y}) + \text{const.} \quad (48)$$

Poisson case. Starting from $\mathcal{L}_{\text{GR2R-MSE}}^\alpha$ with \mathbf{y}_1 constructed in terms of \mathbf{y} , \mathbf{y}_2 and α as $\mathbf{y}_1 = (\mathbf{y} - \mathbf{y}_2\alpha)/(1 - \alpha)$ we have that

$$\mathcal{L}_{\text{GR2R-MSE}}^\alpha(\mathbf{y}; f) = \mathbb{E}_{\mathbf{y}_2|\mathbf{y}} \|f\left(\frac{\mathbf{y} - \mathbf{y}_2\alpha}{1 - \alpha}\right) - \mathbf{y}\|_2^2 - \mathbb{E}_{\mathbf{y}_2|\mathbf{y}} 2 \sum_{i=1}^n (y_{2,i} - y_i) f_i\left(\frac{\mathbf{y} - \mathbf{y}_2\alpha}{1 - \alpha}\right) + \text{const}, \quad (49)$$

evaluating $\lim_{\alpha \rightarrow 0} \mathcal{L}_{\text{GR2R-MSE}}^\alpha(\mathbf{y}; f)$

$$\begin{aligned} \lim_{\alpha \rightarrow 0} \mathcal{L}_{\text{GR2R-MSE}}^\alpha(\mathbf{y}; f) &\propto \lim_{\alpha \rightarrow 0} \mathbb{E}_{\mathbf{y}_2|\mathbf{y}} \|f\left(\frac{\mathbf{y} - \mathbf{y}_2\alpha}{1 - \alpha}\right) - \mathbf{y}\|_2^2 - \lim_{\alpha \rightarrow 0} \mathbb{E}_{\mathbf{y}_2|\mathbf{y}} 2 \sum_{i=1}^n (y_{2,i} - y_i) f_i\left(\frac{\mathbf{y} - \mathbf{y}_2\alpha}{1 - \alpha}\right) \\ &\propto \|f(\mathbf{y}) - \mathbf{y}\|_2^2 + 2 \lim_{\alpha \rightarrow 0} \mathbb{E}_{\mathbf{y}_2|\mathbf{y}} \left(\sum_{i=1}^n y_i f_i\left(\frac{\mathbf{y} - \mathbf{y}_2\alpha}{1 - \alpha}\right) - y_{2,i} f_i\left(\frac{\mathbf{y} - \mathbf{y}_2\alpha}{1 - \alpha}\right) \right) \\ &\propto \|f(\mathbf{y}) - \mathbf{y}\|_2^2 + 2 \sum_{i=1}^n \left(y_i f_i(\mathbf{y}) - \lim_{\alpha \rightarrow 0} \mathbb{E}_{\mathbf{y}_2|\mathbf{y}} y_{2,i} f_i\left(\frac{\mathbf{y} - \mathbf{y}_2\alpha}{1 - \alpha}\right) \right) \end{aligned} \quad (50)$$

Recall that $\mathbf{y} = \gamma\mathbf{z}$ and $\mathbf{y}_2 = \gamma\boldsymbol{\omega}/\alpha$ with $\boldsymbol{\omega} \sim \text{Bin}(\mathbf{z}, \alpha)$. Defining the function $g_{i,\alpha} : \omega_i \mapsto f_i\left(\frac{\mathbf{y} - \gamma\boldsymbol{\omega}}{1 - \alpha}\right)$, we have that the second term is

$$\lim_{\alpha \rightarrow 0} \mathbb{E}_{\mathbf{y}_2|\mathbf{y}} y_{2,i} f_i\left(\frac{\mathbf{y} - \mathbf{y}_2\alpha}{1 - \alpha}\right) = \lim_{\alpha \rightarrow 0} \mathbb{E}_{\boldsymbol{\omega}_{-i}|y_i} \mathbb{E}_{\omega_i|y_i} \gamma \frac{\omega_i}{\alpha} f_i\left(\frac{\mathbf{y} - \gamma\boldsymbol{\omega}}{1 - \alpha}\right) \quad (51)$$

$$= \lim_{\alpha \rightarrow 0} \sum_{k=1}^{z_i} \gamma \binom{z_i}{k} \alpha^{k-1} (1 - \alpha)^{z_i - k} k \mathbb{E}_{\boldsymbol{\omega}_{-i}|y_i} g_{i,\alpha}(k) \quad (52)$$

$$= \lim_{\alpha \rightarrow 0} \left(\gamma z_i (1 - \alpha)^{z_i - 1} \mathbb{E}_{\boldsymbol{\omega}_{-i}|z_i} g_{i,\alpha}(1) + \sum_{k=2}^{z_i} \gamma \binom{z_i}{k} \alpha^{k-1} (1 - \alpha)^{z_i - k} k \mathbb{E}_{\boldsymbol{\omega}_{-i}|y_i} g_{i,\alpha}(k) \right) \quad (53)$$

$$\propto \lim_{\alpha \rightarrow 0} \left(\gamma z_i (1 - \alpha)^{z_i - 1} \mathbb{E}_{\boldsymbol{\omega}_{-i}|y_i} g_{i,\alpha}(1) + \mathcal{O}(\alpha) \right) \quad (54)$$

$$\propto \gamma z_i \lim_{\alpha \rightarrow 0} \mathbb{E}_{\boldsymbol{\omega}_{-i}|y_i} g_{i,0}(1) \quad (55)$$

$$\propto y_i f_i(\mathbf{y} - \gamma \mathbf{e}_i), \quad (56)$$

where $\mathbf{e}_i \in \mathbb{R}^n$ is the vector with i -th entry in 1 and with all others in 0. Thus, plugging in this result, we have

$$\lim_{\alpha \rightarrow 0} \mathcal{L}_{\text{GR2R-MSE}}^\alpha(\mathbf{y}; f) = \|f(\mathbf{y}) - \mathbf{y}\|_2^2 + 2 \sum_{i=1}^n y_i \left(f_i(\mathbf{y}) - f_i(\mathbf{y} - \gamma \mathbf{e}_i) \right) + \text{const}. \quad (57)$$

Gamma case. Based on the proposed re-corrution procedure for the Gamma case, we have that the re-corrution of \mathbf{y}_2 in terms of \mathbf{y} and the extra noise $\boldsymbol{\omega} \sim \text{Beta}(\ell\alpha, \ell(1 - \alpha))$ as

$$\mathbf{y}_2 = \frac{\boldsymbol{\omega}}{\alpha} \mathbf{y} \quad (58)$$

then, replacing in the expression of $a_k(y_i)$ for one element y_2, y

$$\begin{aligned} a_k(y) &= \lim_{\alpha \rightarrow 0} \mathbb{E}_{y_2|y,\alpha} \left\{ (y_2 - y) (\alpha y_2)^k \right\} = \lim_{\alpha \rightarrow 0} \mathbb{E}_{\boldsymbol{\omega}|y,\alpha} \left\{ \left(\frac{\boldsymbol{\omega}}{\alpha} y - y \right) (\boldsymbol{\omega} y)^k \right\} \\ &= \lim_{\alpha \rightarrow 0} \mathbb{E}_{\boldsymbol{\omega}|\alpha} \left\{ \frac{\boldsymbol{\omega}^{k+1}}{\alpha} y^{k+1} - \boldsymbol{\omega}^k y^{k+1} \right\} \\ &= y^{k+1} \lim_{\alpha \rightarrow 0} \left(\frac{1}{\alpha} \mathbb{E}_{\boldsymbol{\omega}|\alpha} \{ \boldsymbol{\omega}^{k+1} \} - \mathbb{E}_{\boldsymbol{\omega}|\alpha} \{ \boldsymbol{\omega}^k \} \right) \end{aligned} \quad (59)$$

The k th moment of ω can be expressed recursively as

$$\mathbb{E}\{\omega^{k+1}\} = \frac{\ell\alpha + k - 1}{\ell + k - 1} \mathbb{E}\{\omega^k\} \quad (60)$$

then

$$\lim_{\alpha \rightarrow 0} \left(\frac{1}{\alpha} \mathbb{E}_{\omega|\alpha}\{\omega^{k+1}\} - \mathbb{E}_{\omega|\alpha}\{\omega^k\} \right) = \lim_{\alpha \rightarrow 0} \mathbb{E}_{\omega|\alpha}\{\omega^k\} \left(\frac{1}{\alpha} \frac{\ell\alpha + k - 1}{\ell + k - 1} - 1 \right) \quad (61)$$

$$= \lim_{\alpha \rightarrow 0} \mathbb{E}_{\omega|\alpha}\{\omega^k\} \frac{\ell\alpha + k - 1 - \alpha(\ell + k - 1)}{\alpha(\ell + k - 1)} \quad (62)$$

$$= \lim_{\alpha \rightarrow 0} \mathbb{E}_{\omega|\alpha}\{\omega^k\} \frac{(k-1)(1-\alpha)}{\alpha(\ell + k - 1)} \quad (63)$$

$$= \lim_{\alpha \rightarrow 0} \left(\prod_{r=0}^{k-1} \frac{\alpha\ell + r}{\ell + r} \right) \frac{(k-1)(1-\alpha)}{\alpha(\ell + k - 1)} \quad (64)$$

$$= \lim_{\alpha \rightarrow 0} \left(\prod_{r=1}^{k-1} \frac{\alpha\ell + r}{\ell + r} \right) \frac{\alpha\ell (k-1)(1-\alpha)}{\ell \alpha(\ell + k - 1)} \quad (65)$$

$$= \lim_{\alpha \rightarrow 0} \left(\prod_{r=1}^{k-1} \frac{\alpha\ell + r}{\ell + r} \right) \frac{(k-1)(1-\alpha)}{(\ell + k - 1)} \quad (66)$$

$$= \left(\prod_{r=1}^{k-1} \frac{r}{\ell + r} \right) \frac{(k-1)}{(\ell + k - 1)} \quad (67)$$

$$= \frac{(k-1)! \Gamma(\ell)}{\Gamma(\ell + k)} \frac{\ell(k-1)}{(\ell + k - 1)} \quad (68)$$

$$(69)$$

Finally, substituting $a_k(y_i)$ in (42) for the Gamma case we have that

$$\lim_{\alpha \rightarrow 0} \mathcal{L}_{\text{GR2R-MSE}}^\alpha(\mathbf{y}; f) = \|\mathbf{f}(\mathbf{y}) - \mathbf{y}\|_2^2 + 2 \sum_{i=1}^n \sum_{k \geq 1} \frac{\ell(k-1)}{k(\ell + k - 1)} \frac{(-y_i)^{k+1} \Gamma(\ell)}{\Gamma(\ell + k)} \frac{\partial^k f_i}{\partial y_i^k}(\mathbf{y}) + \text{const.} \quad (70)$$

C Experimental details

The maximum-entropy sampling strategy, detailed below, is employed to generate noise that ensures the third moment is preserved in the experiment described in Section 4.1. Non-Gaussian Additive Noise, in the main paper.

C.1 Maximum-entropy sampling

Consider a random variable z with $\mu_i = \mathbb{E} z^i$ the desired moments of order $i = 1, \dots, k$. We obtain maximum entropy samples verifying the desired moments up to order k by minimizing [30]

$$\arg \min_{\mathbf{z}} \sum_{i=0}^k \left\| \frac{1}{n} \sum_{j=1}^n z_j^i - \mu_i \right\|_2^2 \quad (71)$$

via gradient descent where we initialize $\mathbf{z} \sim \mathcal{N}(\mu_1 \mathbf{1}, \mathbf{I}(\mu_2 - \mu_1^2))$. The optimization is stopped when the relative error is small, i.e.,

$$\frac{\frac{1}{n} \left| \sum_{j=1}^n z_j^i - \mu_i \right|}{|\mu_i|} < 0.1$$

for all $i = 1, \dots, k$.

D Additional Simulations and Results

D.1 Effect of the re-corruption hyper-parameter α .

We evaluate the performance of the proposed GR2R loss on the PSNR metric when examining the effect of the re-corruption parameter α on three noise distributions: Poisson, Gamma, and Gaussian. Specifically, the experimental setup consists of training the DnCNN model architecture by minimizing the proposed loss $\mathcal{L}_{\text{GR2R-MSE}}^\alpha$ for different values of α on the DIV2K dataset. All experiments share the same training configuration: Adam optimizer, with an initial learning rate of $1e-4$ and 250 training epochs. For the noise model parameters, we set $\gamma = 0.5$ for the Poisson experiment, $\ell = 5$ for the Gamma experiment, and $\sigma = 0.1$ for the Gaussian experiment.

We test the GR2R loss for α values in the interval $[0.1, 3.5]$ for Poisson and Gamma and in the interval $[0.1, 0.9]$ for Gaussian. A scatter plot is shown in Figure 5 for all noise distributions tested, with the trends highlighted by polynomial fitting. A trade-off between the value of α and the PSNR score can be observed, where low values of α indicated less SNR in \mathbf{y}_1 and higher SNR in \mathbf{y}_2 . For the Poisson and Gamma distributions, the optimal values of the re-corruption parameter α appear to be approximately $\alpha = 0.12$, while for the Gaussian distribution, the preferred value seems to be $\alpha = 0.3$. Furthermore, although the performance of the GR2R loss is sensitive to the choice of the re-corruption parameter α . The disparity between the highest and lowest PSNR scores is less than 0.2 dB for the Gamma and Gaussian distributions and less than 0.6 dB for Gaussian noise.

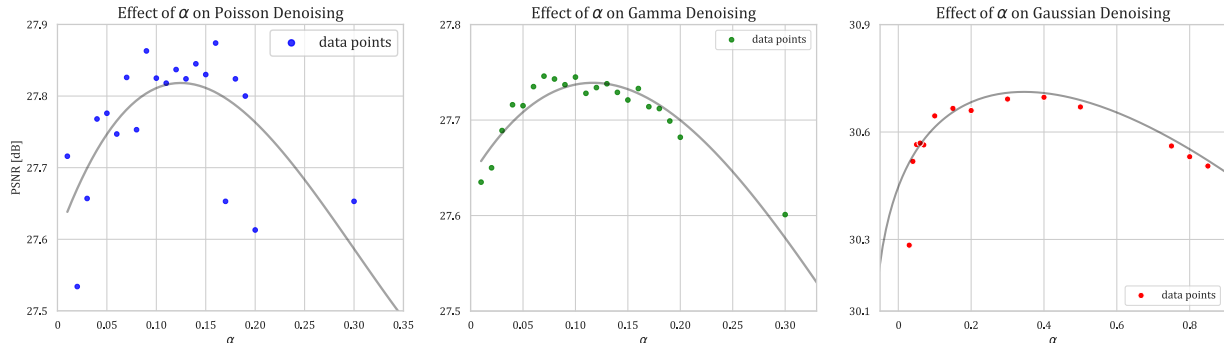


Figure 5: Effect of α parameter for different noise distributions. The results indicate that the optimal α parameter consistently lies within the range of 0.1 to 0.3 across all tested scenarios.

D.2 Log-Rayleigh Noise

In addition to the numerical comparisons presented in the main manuscript between R2R (matching second-order moment) and the proposed GR2R (matching third-order moment), presented in Section 4.1 in the main document, this section offers further elaboration on the experimental setups, as well as visual analyses of the noise estimation compared to the restored images. The training configuration consists of the DnCNN model along 100 epochs with a batch size of 15 with an initial learning rate of $5e-4$ with the Adam optimizer in the DIV2K dataset. Figure 6 displays a histogram comparing the original Log-Rayleigh noise, which was utilized to corrupt the images, with the estimated additional noise provided by R2R and GR2R. It can be observed that extending the moment matching to the third moment significantly enhances the accuracy of the noise distribution estimation compared to matching only until the second moment. Restored images are presented in Figure 7, which demonstrate the effect of matching the third moment in image denoising.

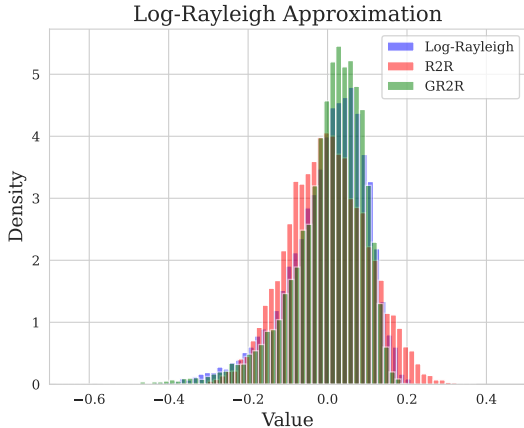


Figure 6: Histogram of noise estimations.

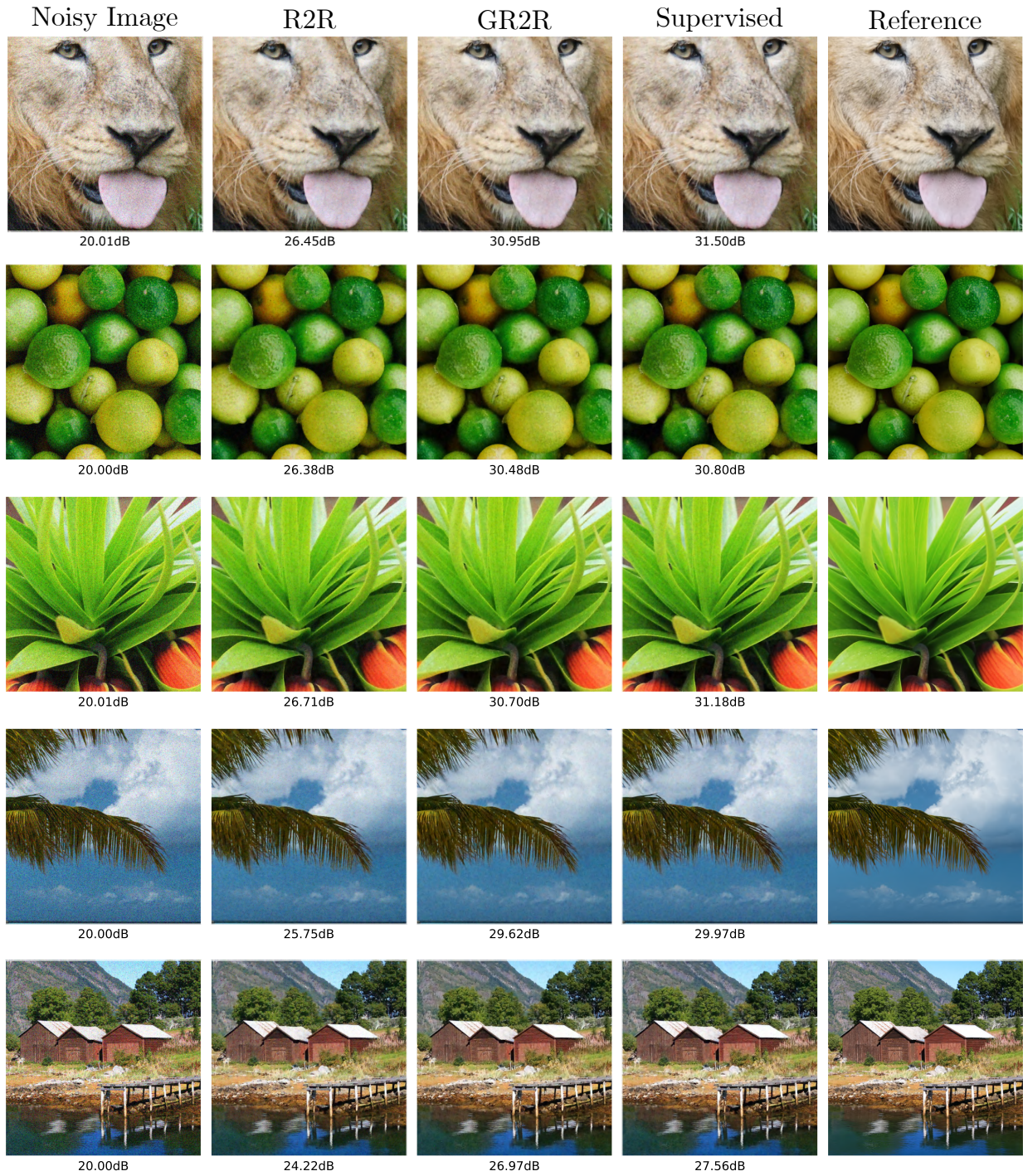


Figure 7: Visual Results for a Log-Rayleigh Noise with a standard deviation of $\sigma = 0.1$.

D.3 Additional Results

The following subsections present results of the PSNR mean and standard deviation obtained for the different methods for Poisson, Gamma, and Gaussian distributions. Each subsection also shows additional visual results.

D.3.1 Poission Noise

Table 7: PSNR results on Poission noise. GR2R-NLL stands for the proposed GR2R with Negative Log-Likelihood.

Poisson Noise Noise Level (γ)	Methods				
	PURE [13]	Neigh2Neigh [20]	GR2R-NLL (ours)	GR2R-MSE (ours)	Supervised-MSE
0.01	32.69±2.13	33.37±2.20	33.90±2.26	33.92±2.20	33.96±2.23
0.1	24.37±1.89	28.27±2.60	28.30±2.65	28.35±2.64	28.39±2.65
0.5	22.98±1.53	24.90±2.68	25.07±2.71	24.69±2.74	25.32±2.75
1.0	17.94±1.13	23.56±2.67	23.69±2.70	23.49±2.71	23.85±2.72

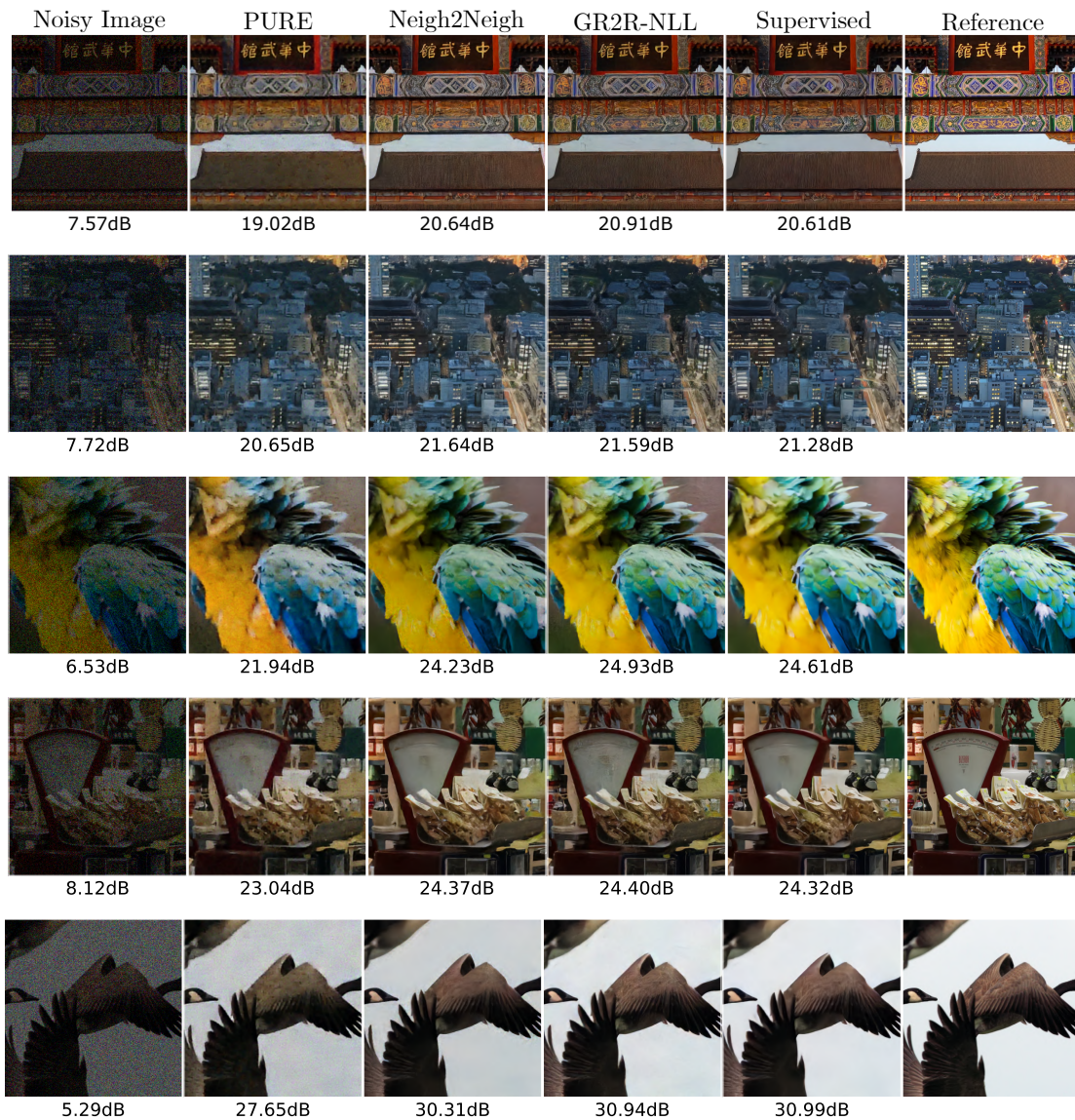


Figure 8: Poission Denoising in DIV2K Dataset.

D.3.2 Gamma Noise

Table 8: PSNR results on Gamma noise. GR2R-NLL stands for the proposed GR2R with Negative Log-Likelihood.

Gaussian Noise Number of looks (ℓ)	Methods			
	Neigh2Neigh [20]	GR2R-NLL (ours)	GR2R-MSE (ours)	Supervised-MSE
30	30.34±1.60	30.43±1.61	31.58±1.72	31.86±1.73
15	28.56±1.58	28.71±1.59	29.55±1.68	29.76±1.70
5	25.71±1.53	25.79±1.49	26.35±1.57	26.72±1.62
1	22.19±1.40	22.19±1.34	22.38±1.40	22.56±1.44

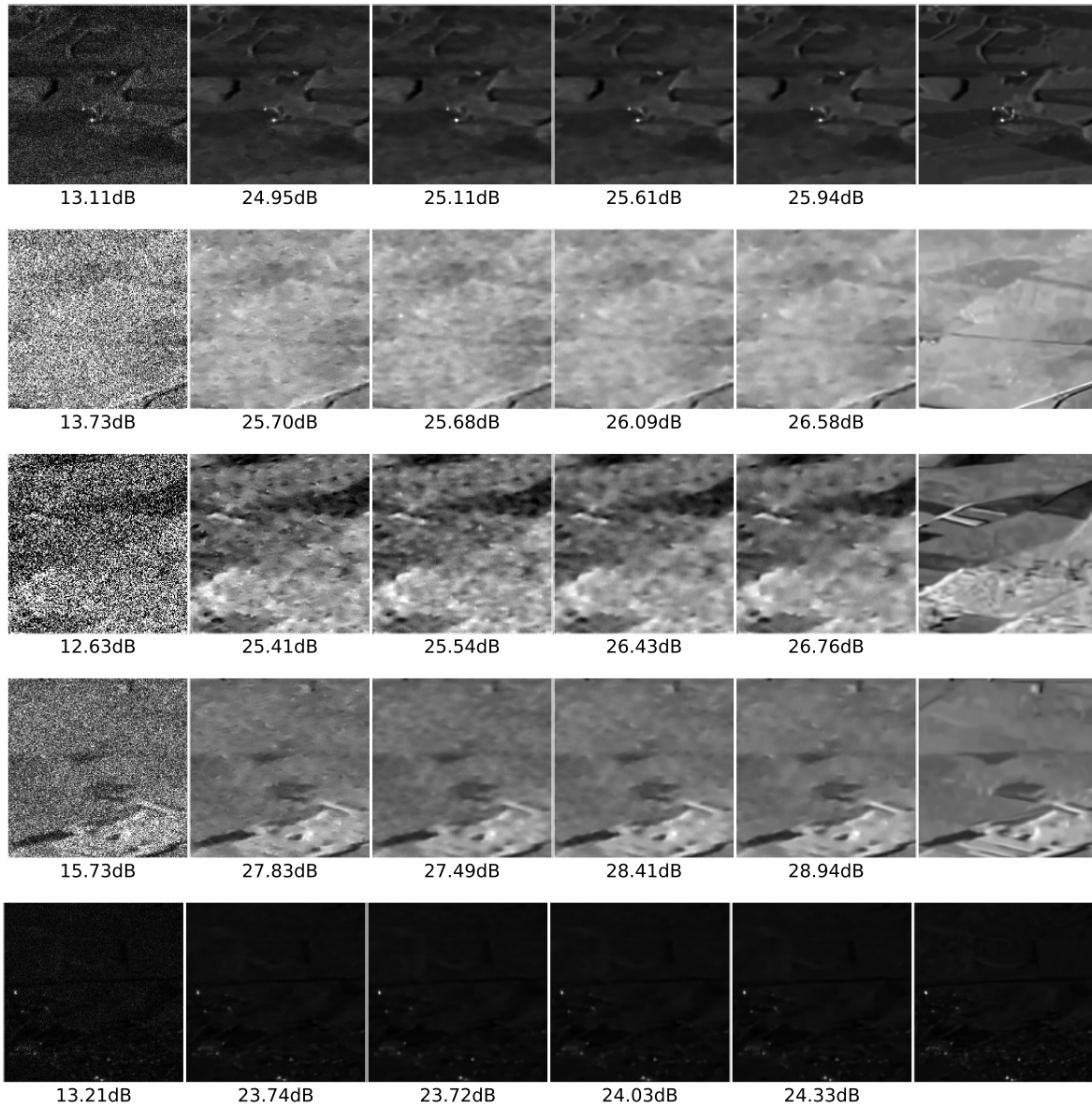


Figure 9: Gamma Denoising in SARDataset.

D.3.3 Gaussian Noise

Table 9: PSNR results for Gaussian noise. For this case, the MSE and NLL variants of GR2R are the same.

Gaussian noise Noise Level (σ)	Methods				
	Noise2Score [25]	SURE [14]	Neigh2Neigh [20]	GR2R (ours)	Supervised-MSE
0.05	34.42±1.16	35.31±1.43	35.07±1.41	35.38±1.47	35.41±1.47
0.1	31.02±0.74	32.76±1.22	32.57±1.22	33.03±1.29	33.14±1.28
0.2	29.34±0.62	29.77±1.02	29.73±1.05	30.24±1.05	30.38±1.05
0.5	22.94±0.65	25.52±1.02	25.61±0.99	25.81±0.97	25.93±0.94

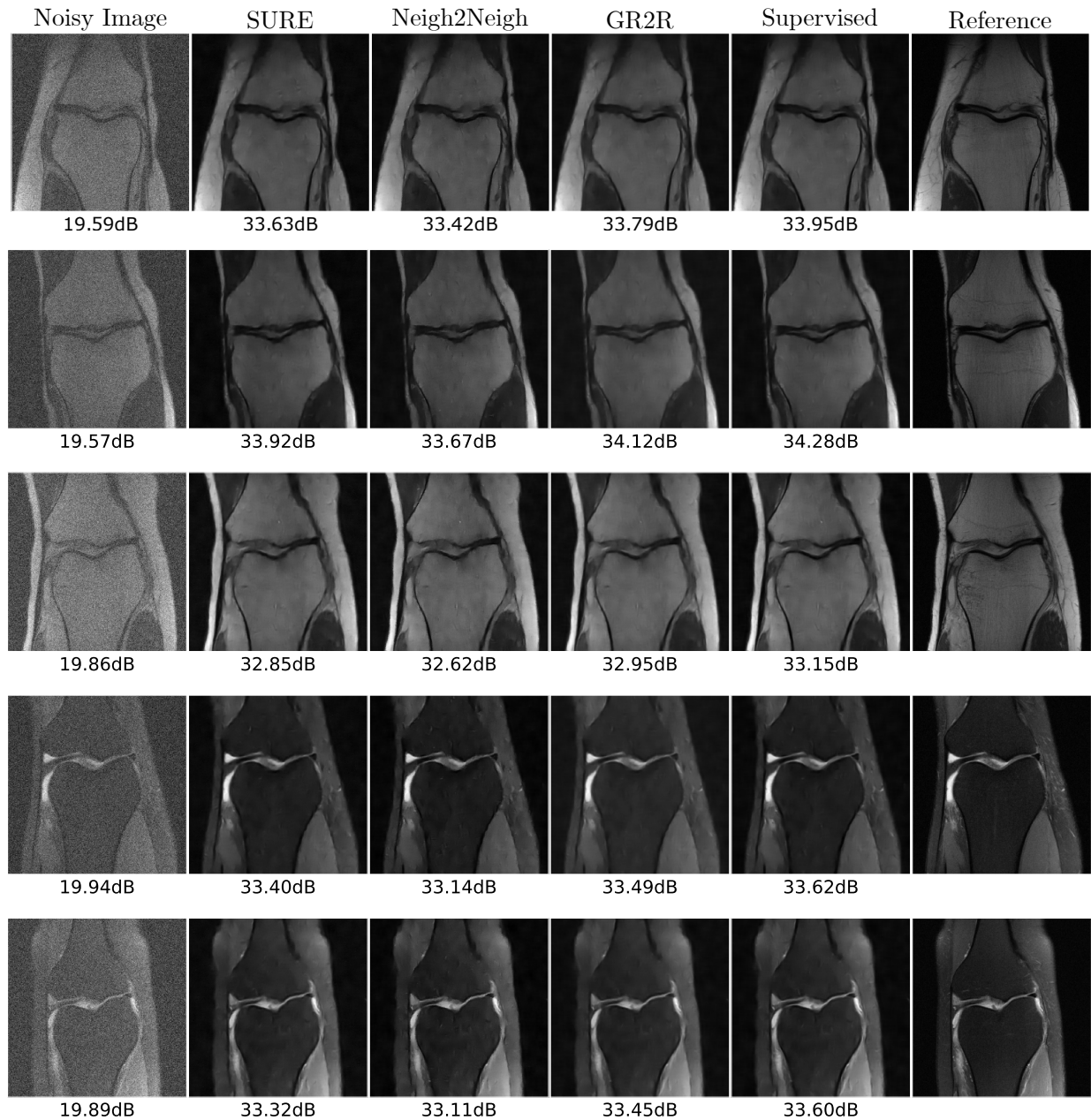


Figure 10: Gaussian Denoising in MRI Dataset.

E General Inverse Problems

This section extends the results of the self-supervised inpainting (Section 5 of the main paper) for Poisson, Gamma, and Gaussian using DIV2K Dataset.

Table 10: PSNR/SSIM results for different noise models on inpainting in DIV2K dataset.

Noise Model	Methods			
	EI [33]	REI [34]	GR2R (ours)	Supervised-MSE
Poisson $\gamma = 0.5$	22.53/0.627	27.05/0.777	27.41/0.791	28.42/0.832
Gamma $\ell = 5$	17.06/0.467	-	26.81/0.784	27.12/0.802
Gaussian $\sigma = 0.1$	23.68/0.671	29.53/0.853	29.58/0.854	29.93/0.866

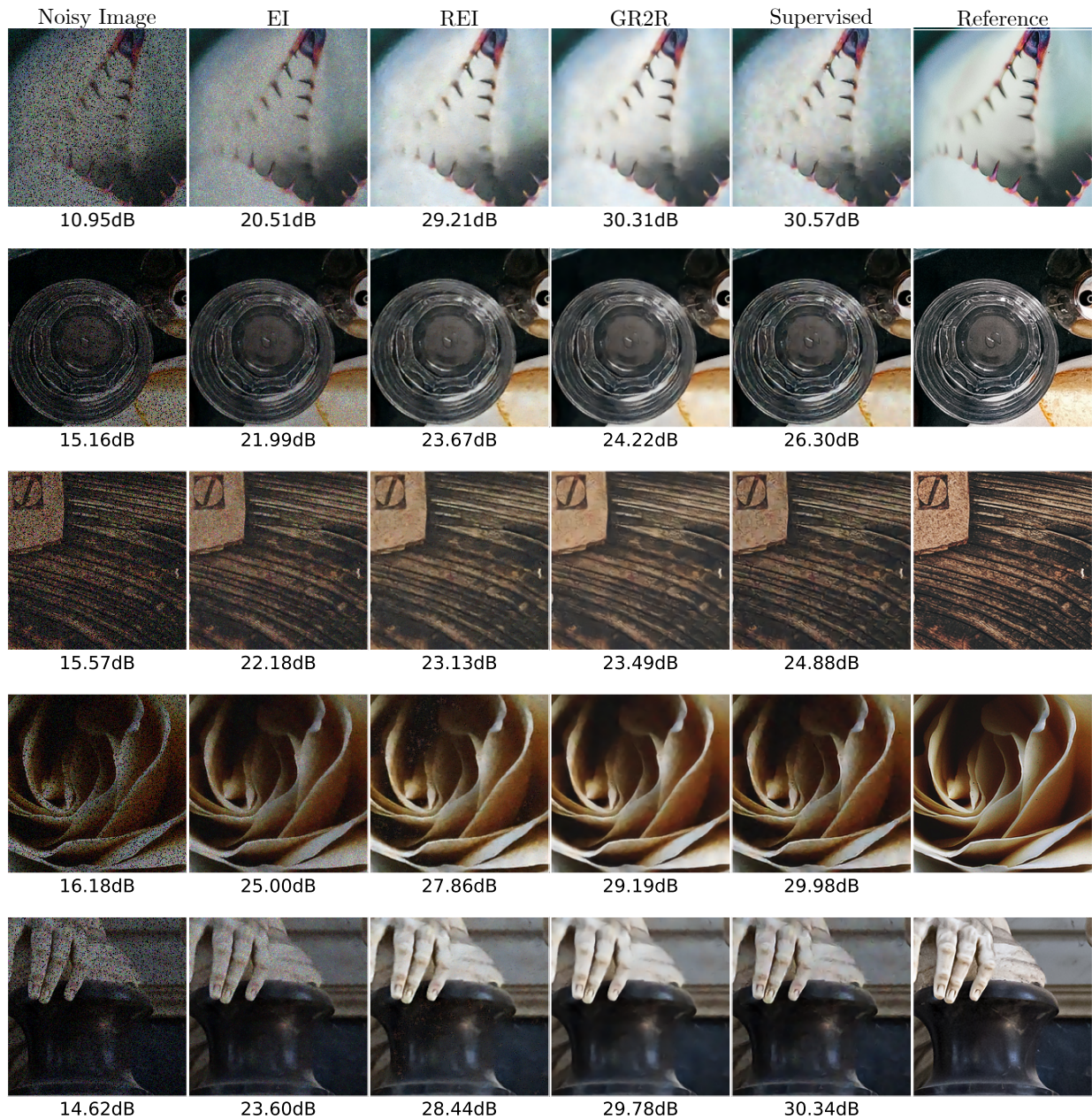


Figure 11: Inpainting with Poisson noise in DIV2K Dataset.

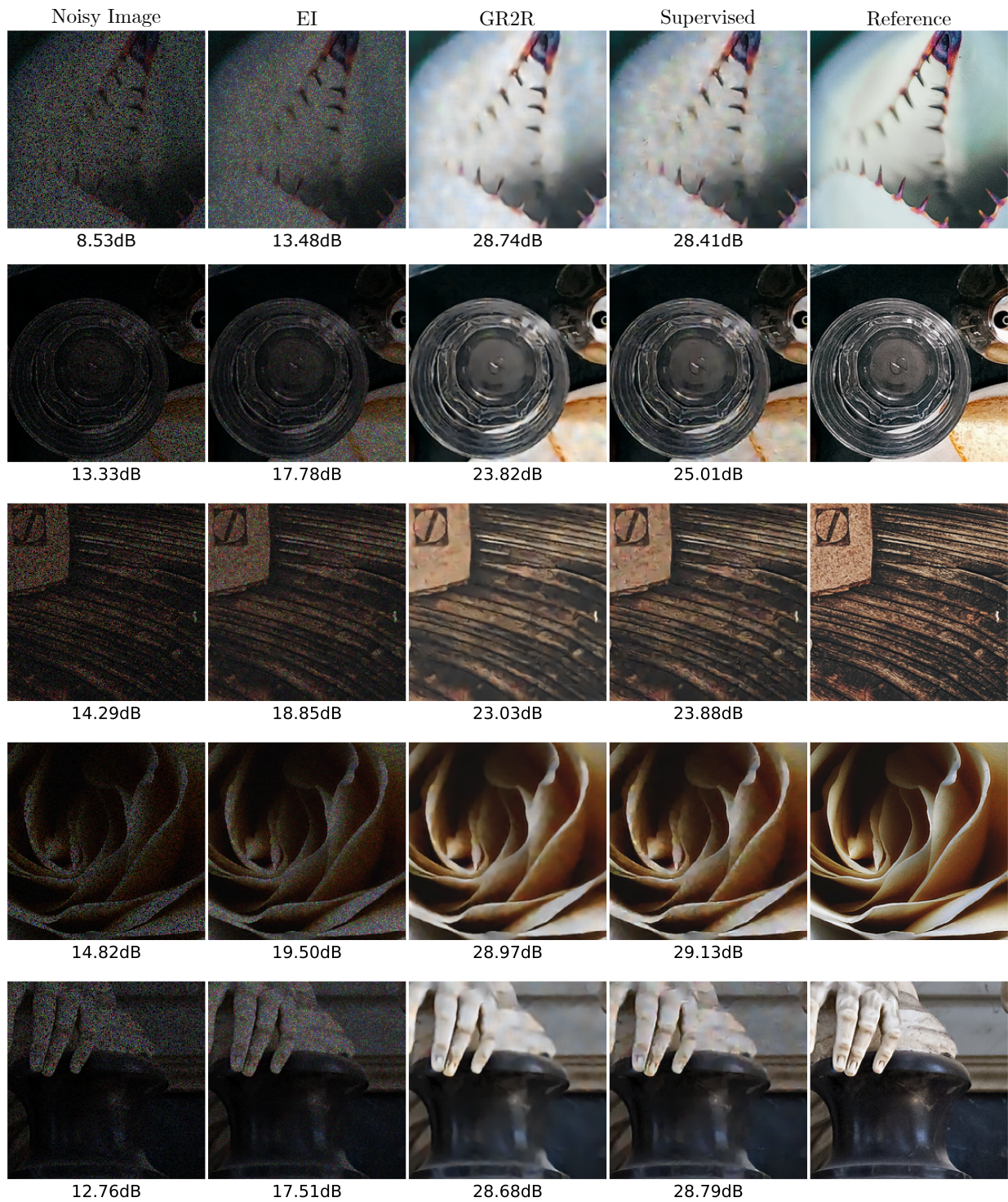


Figure 12: Inpainting with Gamma noise in DIV2K Dataset.

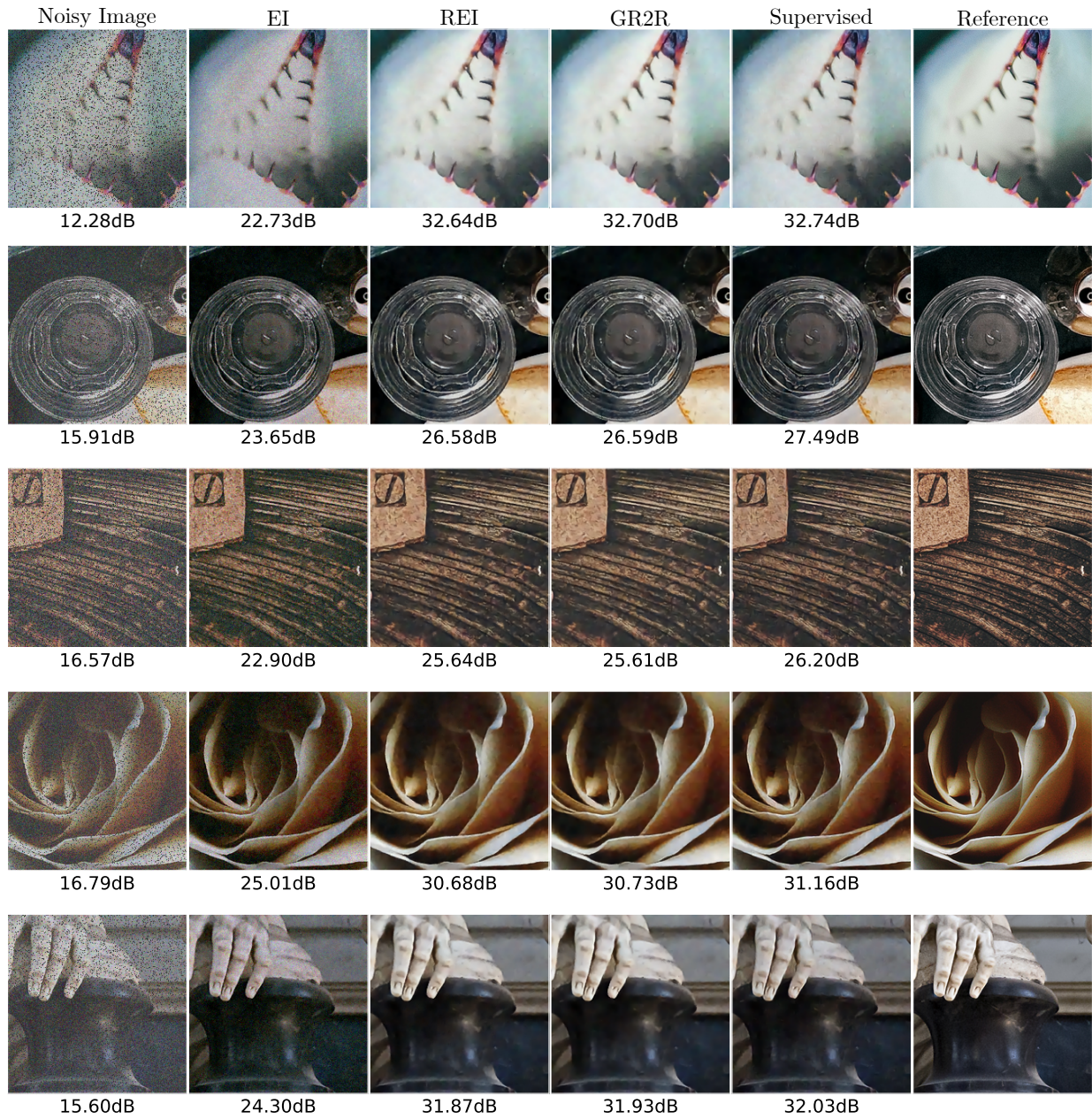


Figure 13: Inpainting with Gaussian noise in DIV2K Dataset.